An Experimental and Theoretical Study of the Self-Assembly of Gold Nanoparticles at the Surface of Functionalized Multiwalled Carbon Nanotubes

Toby Sainsbury, Jacek Stolarczyk, and Donald Fitzmaurice*

Department of Chemistry, University College Dublin, Belfield, Dublin 4, Ireland

Received: March 9, 2005; In Final Form: June 19, 2005

This paper reports the findings of a detailed study of the self-assembly of gold nanoparticles at the surface of carbon nanotubes (CNTs). The study included the development of a predictive model for the interactions (charge transfer, van der Waals, osmotic, elastic, nonelastic, and covalent) between tetraoctylammonium bromide-stabilized (TOAB) gold nanoparticles and alkyl- and alkylthiol-modified multiwalled carbon nanotubes (MWCNTs). It also included the measurement of the coverage of gold nanoparticles at the surface of the above MWCNTs as a function of increasing alkyl chain length. One key finding is that it is possible to predict with a high degree of accuracy using the above model the measured coverage of gold nanoparticles adsorbed, either noncovalently or covalently, at the surface of a MWCNT. Another key finding is that, as predicted, under well-defined conditions the measured coverage of nanoparticles is very sensitive to the nature of the modified CNT surface and the contiguous environment, providing valuable insights that will underpin the rational design of functional nanoscale devices assembled from nanoparticle and CNT building blocks.

Introduction

The inherent limitations of existing top-down approaches to the fabrication of functional nanoscale architectures, described elsewhere,[1] have led to the growth of interest in alternative, bottom-up approaches. When considering possible bottom-up approaches, many researchers have been attracted to the use of nanoparticles and carbon nanotubes (CNTs) as building blocks and to their assembly in solution and organization at patterned substrates.[2,3]

The attraction to nanoparticles as nanoscale building blocks is a consequence of the increasing availability of dispersions of sterically stabilized and similarly sized and shaped metal, semiconductor, and insulator nanoparticles whose properties are dominated by confinement and surface effects and are therefore size-tunable.[4,5] It is also a consequence of the increasing availability of stabilizing ligands, which incorporate functional groups or receptor−substrate sites, that can be used to chemically modify nanoparticles or program their interaction with other molecules, nanoparticles, nanotubes, or substrates.[6,7] Not surprisingly, nanoparticles are finding an increasing number of commercial applications in the electronic, photonic, pharmaceutical, medical device, agri-food, construction, environmental, material science, and engineering sectors.[8,9]

The attraction to CNTs is a consequence of the increasing availability of high-purity samples of single-walled carbon nanotubes (SWCNTs) and multiwalled CNTs (MWCNTs) of well-defined diameters and lengths, with correspondingly well-defined electronic and mechanical properties.[10] It is also a consequence of the increasingly rich chemistry, which can be used to attach the molecules to the ends or sidewalls of CNTs.[11,12] Although not explored as extensively as is the case of nanoparticles, this chemistry also offers the prospect of modifying the surface of CNTs with molecules incorporating functional groups or receptor−substrate sites. Consequently, CNTs have found applications in a number of technologically relevant disciplines such as electronics, catalysis, materials science, and sensing applications.[13]

It is noted that there are already several reports that have demonstrated the use of nanoparticles or CNTs as building blocks for functional nanoscale devices.[14] It is also noted that there are relatively few reports describing the combined use of nanoparticles and CNTs.[15−17]

In addition to these reports, we have recently described the use of unmodified and modified MWCNTs to template the noncovalent and covalent assembly of metal, semiconductor, and insulator nanoparticles.[18−20] Notably, we have also reported the use of alkylthiol-modified MWCNTs to covalently template the assembly of gold nanoparticles, which were subsequently enlarged and enjoined by electroless deposition to form a continuous polycrystalline gold nanowire. The resistivity of the resulting gold nanowire has been measured and found to be of the order of 10^{-4} Ω m.[21] Our current efforts are, in part, focused on patterning MWCNTs so that they can be used to template the assembly of more complex and highly functional nanoscale architectures and, in part, focused on organizing these MWCNT templates on conventionally patterned substrates, ultimately allowing the above functional nanoscale architectures to be addressed and integrated.

To fully realize the potential of nanoparticles and CNTs as building blocks for functional nanoscale architectures, it will be essential to understand the interactions between nanoparticles and CNTs and to exploit this understanding to rationally design and assemble in solution functional nanoparticle−CNT architectures and to organize these nanoscale architectures at patterned substrates.

While the interactions between nanoparticles and CNTs have been addressed only in a descriptive manner,[16,22] significant progress has been made in the rigorous analysis of nanoparticle−nanoparticle interactions. In one report, Korgel et al. have shown that the balance between the attractive van der Waals interaction between nanoparticle cores and the steric repulsion of the stabilizing ligands determines the ordering of dodecanethiol-

* Corresponding author. E-mail: donald.fitzmaurice@ucd.ie.

10.1021/jp051224c CCC: $30.25
Published on Web 08/06/2005

SCHEME 1: Templated Assembly of TOAB-Stabilized Gold Nanoparticles at the Surface of Unmodified, Alkyl-Modified, and Alkylthiol-Modified MWCNTs (PA-, PTA-, OA-, DDA-, MEA-, MHO-, and MUDO-MWCNTs)

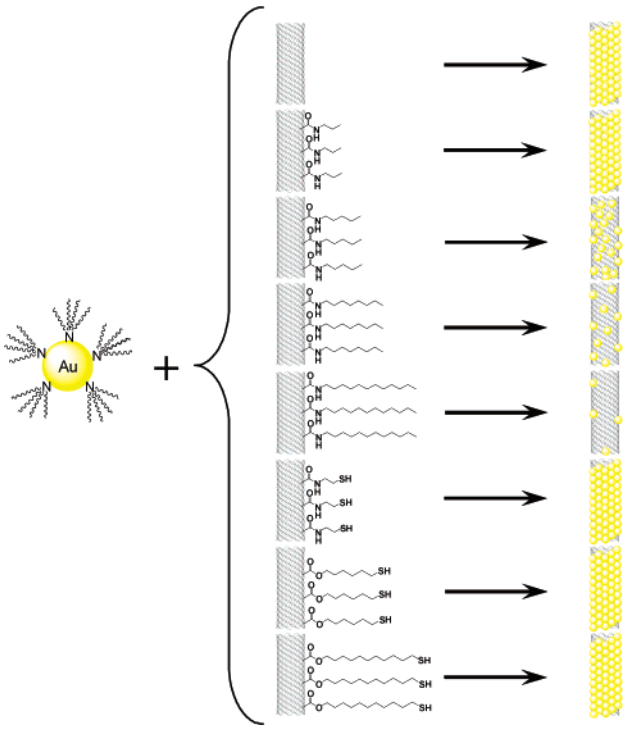

stabilized gold nanoparticles.[23,24] These results led to the development of a "soft sphere" model, which could account for the interdigitation of the ligand chains.[24] In a further development, steric stabilization by the ligand at the surface of the nanoparticle has been evaluated to explain the size and polydispersity of silver nanoparticles obtained during a growth process in supercritical CO_2.[25]

It is in this context that the findings of a detailed study of the self-assembly of gold nanoparticles at the surface of CNTs are reported here. A quantitative model for interactions (charge transfer, van der Waals, osmotic, elastic, nonelastic, and covalent) between ligand-stabilized nanoparticles and modified MWCNTs has been developed and used to predict the coverage of the CNT by gold nanoparticles for a range of different experimental conditions. To verify these predictions, MWCNTs have been covalently modified with alkyl and alkylthiol chains of increasing length and have been combined in solution with tetraoctylammonium bromide (TOAB)-stabilized gold nanoparticles, according to Scheme 1. This approach provided the means to study both the noncovalent and covalent (for alkyl- and alkylthiol-modified MWCNTs, respectively) adsorption of gold nanoparticles at the surface of MWCNTs. The coverage of gold nanoparticles at the surface of the MWCNTs was subsequently determined using transmission electron microscopy (TEM). The results were found to be fully consistent with the predictions of the theoretical model.

Dodecanethiol (DDT) is known to easily replace other, relatively weakly bound ligands which stabilize gold nanoparticles, due to the high affinity of the thiol group to gold surfaces.[26] Therefore, it was interesting to study the nanoparticle−CNT interactions when the assembly was treated with DDT. This experiment was also designed to further test the viability of the assumptions of the model.

The aim of the work was therefore two-fold: (i) to characterize the self-assembly of gold nanoparticles at the surface of alkyl- and alkylthiol-modified MWCNTs and (ii) to develop a predictive, quantitative model of the interactions which could provide valuable insights into the nature of the interactions and may help to better control the self-assembly process.

SCHEME 2: Illustration of the Geometry of Interactions between an Alkyl- and Alkylthiol-Modified MWCNT and a TOAB-Stabilized Gold Nanoparticle

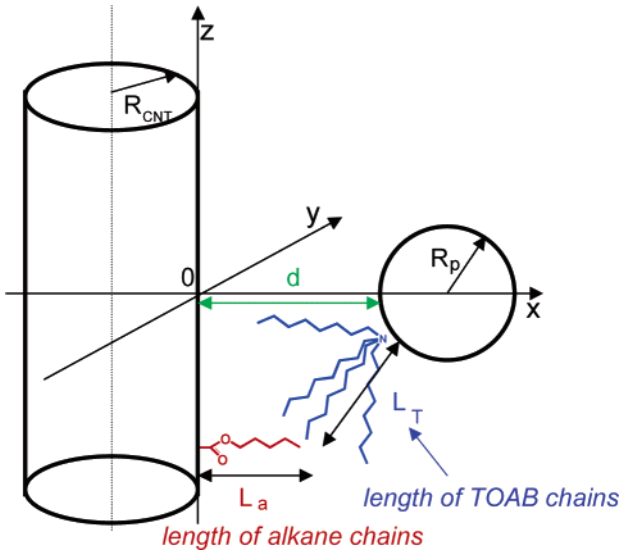

Theory

Model Outline. Several models have been formulated to describe the interactions between the ligand-stabilized nanoparticles.[24,27−29] These models were partially based on Derjaguin−Landau−Verwey−Overbeek (DLVO) theory, which has been widely used to analyze the interactions between colloidal particles with adsorbed layers and their effect on the stability of colloidal dispersions.[30−32] DLVO theory assumes that the separation between the particles is controlled by the balance between van der Waals attractive force and repulsive electrostatic double layer potential enhanced by the steric hindrance of the adsorbed layer.[33]

However, the problem of interactions between a modified multiwalled carbon nanotube and ligand-stabilized gold nanoparticles, analyzed in this paper, presents a number of new challenges, which cannot be directly addressed using any of the models referred to above. Specifically, the major issues are as follows: (i) the geometry of the interactions between a cylinder (nanotube) and a sphere (nanoparticle); (ii) the radii of curvature of the surfaces are comparable with the thickness of the ligand layers which may invalidate the widely used Derjaguin approximation;[33] (iii) analysis of the effect of varying the length of the ligands coupled with the nanotube or stabilizing the nanoparticle requires a model that could account for different ligands on both interacting objects; (iv) an additional attractive term due to charge transfer between a nanoparticle and a nanotube is important but has not previously been considered in detail either by us or others.[18,34]

Therefore, to account for the adsorption of TOAB-stabilized gold nanoparticles at the surface of alkyl- and alkylthiol-modified MWCNTs, a new model has been developed, which examines in detail the interaction between a single MWCNT and a nanoparticle, as a function of the distance separating the two (see Scheme 2). The approach adopted is analogous to that used in developing DLVO theory. Specifically, it is assumed that the contributions to the total interaction energy are additive.

Hence, the total interaction energy is expressed as a sum of all terms which constitute the model: charge transfer attraction, van der Waals attraction, osmotic repulsion, elastic repulsion, and nonelastic repulsion.

$$E(d) = E_{CT}(d) + E_{vdW}(d) + E_{osm}(d) + E_{elas}(d) + E_{nonelas}(d) \quad (1)$$

It is noteworthy that, although the length of the ligands coupled with MWCNTs does not explicitly appear in eq 1, all of the repulsive components of the model depend on it; thus, the model indirectly depends on this critical experimental parameter.

Due to the comparable thickness of the ligand layers with the radii of both the MWCNT and the nanoparticle, the curvatures of their surfaces must be taken into account when calculating the volume fraction occupied by the ligand chains. Briefly, the chains are modeled as cylinders which extend from the surface; thus, the volume fraction (ϕ) decreases with increasing distance (x) from the surface. Hence, in the case of the nanotube, ϕ can be expressed by eq 2 (Scheme 2):

$$\phi_{CNT}(x) = \frac{\phi_{CNT}(0)R_{CNT}}{R_{CNT} + x} \quad (2)$$

where $\phi_{CNT}(0)$ is the volume fraction of the chains at the surface of the MWCNT. In the case of a TOAB molecule at the surface of a gold nanoparticle, a more complex treatment of the volume fraction occupied by the molecule is necessary, on account of the geometry of the quaternary ammonium salt.[35] For the sake of simplicity, a model of four cylinders of length L_T which extend from the surface of the gold nanoparticle is adopted, as expressed by eq 3 (cf. Scheme 2).

$$\phi_p(x,d) = \frac{\phi_p(0){R_p}^2}{(R_p + d - x)^2} \quad (3)$$

Here, $\phi_p(0)$ is the volume fraction of the chains at the surface of the nanoparticle. The complete derivation of eqs 2 and 3 and necessary assumptions are given in Supporting Information section S1.

Noncovalent Interactions. The van der Waals, osmotic, and elastic terms from eq 1 have all been analyzed for sphere−sphere geometry in previous models;[24,27−29] therefore, they are described here only briefly. The particular expressions and derivations suitable for the cylinder−sphere geometry and the scale of this particular system have been derived and are given in Supporting Information section S3, due to their complexity. The charge transfer attraction and nonelastic repulsion are presented here in detail.

Charge Transfer. Fullam and Fitzmaurice have reported the MWCNT templated self-assembly of TOAB-stabilized gold nanoparticles in solution.[18] In this case, the charge transfer interaction between the conduction band of the gold nanoparticles and the continuum of π^* states present at the surface of the MWCNTs was recognized as an important contribution to the driving force for the adsorption of the gold nanoparticles, based on the previously reported work of others.[34] It was also concluded that the lability of the TOAB ligands at the surface of the gold nanoparticles facilitates the close approach of the materials, allowing a short-range charge transfer interaction to drive the adsorption of the nanoparticles. Here, to enable a quantitative analysis, the distance dependent charge transfer interaction between a gold nanoparticle and a MWCNT is calculated on the basis of the probability of an electron tunneling through the alkane layer between the materials. Assuming a superexchange character of the electron transfer process (i.e., no intermediate states), the amount of charge transferred decays exponentially with distance.[36,37]

$$Q(d) = Q_0 e^{-\lambda d} \quad (4)$$

The amount of charge transferred when the MWCNT and the nanoparticle are in contact is represented by Q_0. The attenuation coefficient for charge transfer (λ) has been experimentally found to be of the order of 0.87 Å^{-1} for saturated hydrocarbon bridges or linkers between an electron donor and acceptor.[37,38]

Using Gauss's law, the expression for the Coulombic electrostatic attraction between alkyl-modified MWCNTs and TOAB-stabilized gold nanoparticles, induced by the charge transfer, can be obtained:

$$E_{CT}(d) = -\frac{1}{4\pi\epsilon\epsilon_0}\frac{Q^2(d)}{R_{CNT} + R_p + d} \quad (5)$$

where $\epsilon = 2$ is the dielectric constant for the saturated hydrocarbon layer (paraffin) and ϵ_0 is the vacuum permittivity.

According to eqs 4 and 5, the charge transfer interaction (E_{CT}) is an exponentially decreasing function of distance (equal to the alkane bridge layer thickness) with an attenuation factor (λ) of twice 0.87 Å^{-1}. Therefore, the charge transfer contribution to the overall interaction between alkyl-modified MWCNTs and TOAB-stabilized gold nanoparticles is relevant only for very small separations, not larger than 0.5 nm. This prediction is consistent with electron transfer quenching and Coulomb blockade effects observed for thiol-passivated silver and gold nanoparticles separated by more than 0.5 ± 0.2 nm.[39−41] A separation of this magnitude corresponds to metal nanoparticles stabilized by self-assembled monolayers of pentanethiol or hexanethiol.[39]

Despite the fact that there have been multiple reports concerning charge transfer interactions between CNTs and gold,[34] a quantitative description of the amount of charge actually transferred between the gold atoms and the nanotube has not been reported to date. Comparative studies have shown that transition metals bind much more strongly than noble metals, such as gold.[42] Charge transfer interactions have also been shown to depend strongly on the radius of nanotubes.[43] For these reasons, the amount of charge transferred (Q_0) (i.e., when the MWCNT and gold nanoparticle are in contact) has been treated in this model as an adjustable parameter. It is important to note, in the case of alkyl-modified MWCNTs, that due to the steric barrier of the alkyl chains the two objects cannot come into contact, and the actual amount of charge transferred is significantly smaller than Q_0.

van der Waals. The van der Waals interaction between a MWCNT and a gold nanoparticle may be approximated by an interaction between a cylinder and a sphere. For reasons given earlier, the Derjaguin approximation is unsuitable for the calculation. Accordingly, an alternative approach called surface element integration (SEI)[44] has been adopted here (see Supporting Information section S2). The value of the Hamaker constant for this system ($A_{CNT-alk-Au}$) is derived from the Hamaker constants for carbon−gold and hydrocarbon−hydrocarbon interactions across a vacuum (A_{CNT-Au} and $A_{alk-alk}$, respectively) using the expression $A_{CNT-alk-Au} = (\sqrt{A_{CNT-Au}} - \sqrt{A_{alk-alk}})^2$.[28,33]

Osmotic. The osmotic repulsion arises from the interdigitation of ligand chains when the distance between a MWCNT and a

nanoparticle is sufficiently small ($d < L_T + L_a$). Consequently, the volumes they are assumed to occupy start to overlap, forcing the exclusion of the solvent molecules. The potential needed to balance the osmotic pressure difference, and hence prevent the influx of solvent particles into the region with a reduced solvent concentration, effectively constitutes an additional repulsive term. This term has been studied extensively by Meier[45] and Napper[30,31] in order to model the steric stabilization of colloidal dispersions by an adsorbed polymeric layer. Their approach, based on the Flory−Huggins theory of free energy of polymer mixing,[46] has been further extended by Vincent et al.[32] and has been used to account for the steric repulsion between nanoparticles covered by alkylthiol monolayers.[28,29] However, due to the different geometry and simplifications of the basic Vincent treatment (constant chain density in the adsorbed layer),[28,29,32,47] direct application of its results is not possible here. Therefore, the appropriate expressions for the osmotic term were derived directly from the work of Meier and Napper[30,31,45] using the SEI technique. The particular details of this derivation, for the sake of clarity, are given in Supporting Information section S3.

Elastic. The elastic term arising from the elastic compression of the ligand chains and their loss of configurational entropy was discussed in detail by Napper et al.[30,31] Here, as was the case for the osmotic term, the expression needed to be derived from the work of Napper to account for a different geometry. The SEI technique was also used here (see Supporting Information section S3).

Nonelastic. The additional repulsive term (called "nonelastic") is necessary, as an alkyl-modified MWCNT and a TOAB-stabilized gold nanoparticle cannot approach each other closer than a distance of the nonelastic limit corresponding to the distance of separation at which the volume fraction of alkyl chains (ϕ) reaches 1. Due, however, to the lability of the TOAB chains, it is assumed that the TOAB chains are easily moved aside and do not contribute to the nonelastic limit distance.[35,48]

It is further assumed that the alkyl chains which are covalently coupled to the modified MWCNTs undergo compression and adopt a close-packing conformation with a tilt (α) of 30° for the chain axis with respect to the MWCNT surface, thereby effectively reducing the nonelastic limit distance. This proposed tilt is analogous to that of alkylthiols on gold surfaces[49] and is further supported by the curvature of a gold nanoparticle, which facilitates moving the alkyl chains outward. Thus, the alkyl chains adopt a highly tilted conformation in order to achieve the optimum packing arrangement, which results in a decrease in the volume fraction of the alkyl chains. Hence, the average volume fraction between the surfaces of the nanotube and the nanoparticle may be expressed by eq 6.

$$\varphi_{av}(d) \cong \frac{1}{d}\int_0^d \phi_{CNT}\frac{L_a}{d}\frac{R_{CNT}}{R_{CNT}+x}\cos\alpha\, dx \qquad (6)$$

The average volume fraction rather than a local volume fraction is used, to allow for possible chain reconfiguration and more efficient packing. The repulsive energy effectively goes to infinity at the nonelastic limit, representing the close approach of the materials. To make the integration with other parts of the model easier, a smoother, continuous function has been chosen, as expressed by eq 7.

$$E_{nonelas}(d) = \exp(k(\phi_{av}(d) - 1)) \qquad (7)$$

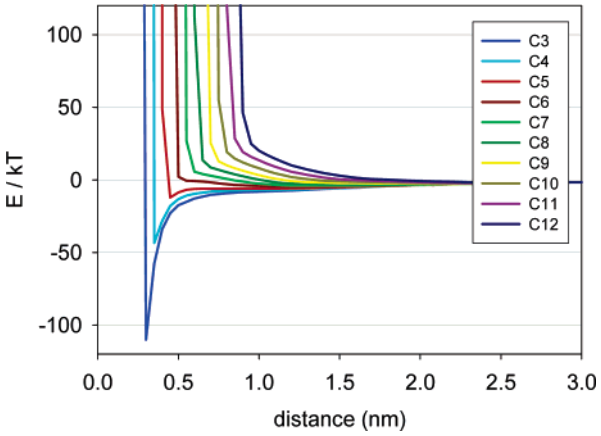

Figure 1. Total potential energy of noncovalent interactions between the alkyl-modified MWCNTs and TOAB-stabilized gold nanoparticles for a range of alkyl chain lengths.

The prefactor in the exponent $k \gg 1$ gives a rapidly increasing function when ϕ_{av} approaches 1.

Having the expressions for each interaction energy term and employing eq 2, the total energy of the interactions between TOAB-stabilized gold nanoparticles and unmodified and alkyl-modified MWCNTs can be calculated as a function of distance. Due to the complexity of the expressions derived using the surface element integration technique, they are evaluated numerically for any separation (d). The length of alkyl chains coupled with MWCNTs (L_a), which is a function of the number of carbon atoms within the chain, is a parameter of all repulsive terms. Hence, a series of the total interaction energy profiles can be obtained using this number as a parameter. The calculated theoretical total interaction energies for a series of alkyl chains containing n carbons (C_n), with n ranging from 3 to 12, are shown in Figure 1.

Covalent Interactions. The modification of MWCNTs with ω-mercapto-derivatives (alkylthiols) offers the possibility of much stronger binding of gold nanoparticles to the surface of nanotubes in comparison with the noncovalent interactions discussed previously. The total interaction in such cases is supplemented and, indeed, dominated by the covalent term arising from the formation of multiple gold−thiol bonds:

$$E(d) = E_{CT}(d) + E_{vdW}(d) + E_{osm}(d) + E_{elas}(d) + E_{nonelas}(d) + E_{Au-S}(d) \qquad (8)$$

The relative lability of a quaternary ammonium ion, when compared with a ligand with a higher affinity for a gold surface, such as a thiol, is known to facilitate the preferential bonding of the more favorable ligand.[48] In the context of this system, the lability of the TOAB ligands at the surface of the TOAB-stabilized gold nanoparticles is believed to allow them to be easily replaced by alkylthiol ligands, which are covalently bound to the surface of the nanotube. The number of covalent bonds, which can be formed between an alkylthiol-modified MWCNT and the surface of a gold nanoparticle, is equal to the number of thiol-terminated alkyl chains ($n_{CNT-thiols}$) that can reach the vicinity (i.e., closer than the average thiol headgroup−gold surface distance[50]) of the surface of the nanoparticle. Such chains can only originate from a small part of the nanotube with surface area A_{CNT} shown in Scheme 3.

The number of chains involved in covalent bond formation can then be calculated by multiplying the surface area (A_{CNT}) by an experimentally known value for the density of carboxylic acid groups at the surface of the MWCNTs (ρ_{COOH}) (eq 9). The

SCHEME 3: Illustration of the Active Surface Area Available for Covalent Au−S Bond Formation at the Surface of Thiol-Modified MWCNTs

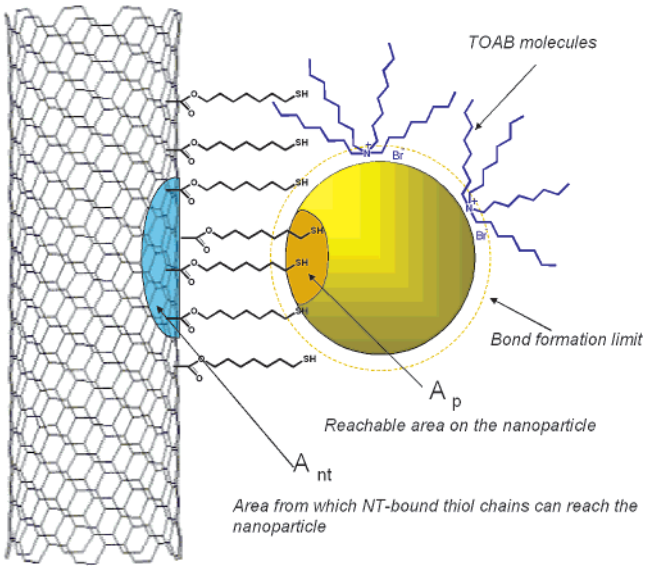

method used to calculate A_{CNT} is shown in Supporting Information section S4.

$$n_{CNT-thiols} = A_{CNT}\rho_{COOH} \quad (9)$$

It is assumed in this case that the thiol chains are parallel to each other. Such orientation allows the thiol chains to interdigitate with the alkyl chains of the TOAB molecules at the surface of the gold nanoparticles. This approach allows a large number of covalent gold−thiol bonds being formed without creating a large steric barrier around the nanoparticle. The total covalent gold−thiol bonding energy between an individual nanoparticle and the surface of the thiol-modified MWCNT can be now described as the number of alkylthiol chains which can theoretically reach the nanoparticle multiplied by the energy per bond (E^{bond}_{Au-S}) and is given by eq 10.

$$E_{cov}(d) = n_{CNT-thiols}(d)E^{bond}_{Au-S} = n_{CNT-thiols}(d)\frac{E^{mol}_{Au-S}}{N_A} \quad (10)$$

Similar to the noncovalent case, the total interaction energy can now be evaluated as a function of distance. The noncovalent terms are evaluated as done previously, with chain lengths (L_a) adjusted for alkylthiols, while the covalent term is evaluated according to eq 10. The contact area (A_{CNT}) is also a function of alkylthiol chain length; hence, the number of carbon atoms in an alkylthiol chain can be used as a parameter of the total interaction energy. Results of such theoretical calculation, shown in Figure 2, are very different from the noncovalent case, proving that the interactions are dominated by the covalent term.

Theoretical Coverage. The model presented here allows the total interaction energy between alkyl-modified MWCNTs and TOAB-stabilized gold nanoparticles to be calculated (see Figures 1 and 2). However, the validation of the theoretical predictions with experimental results, and vice versa, is largely dependent on the ability to determine the coverage of the surfaces of the MWCNTs with gold nanoparticles using transmission electron microscopy (TEM). This may be expressed as a percentage or as a fraction of the total possible coverage. To allow such a comparison between theoretically predicted coverage and experimental values of coverage, two important assumptions

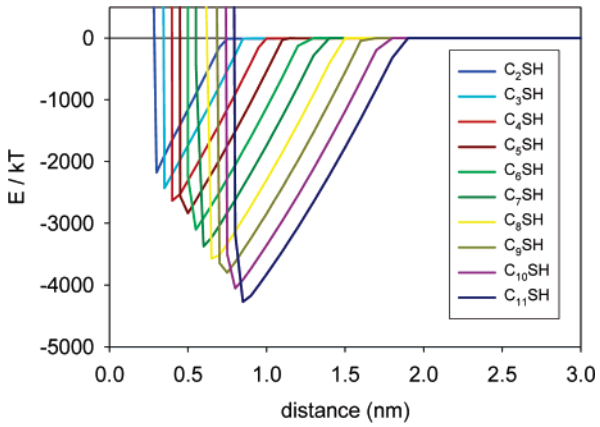

Figure 2. Total potential energy of noncovalent interactions between the alkylthiol-modified MWCNTs and TOAB-stabilized gold nanoparticles for a range of alkylthiol chains.

regarding the arrangement of the nanoparticles must be made: (i) close packing of the nanoparticles is treated as 100% coverage; that is, the unoccupied interstitial space is ignored, as may be seen in Scheme 4a; (ii) lateral mobility of the nanoparticles at the surface of the nanotube ensures that the closest possible packing is achieved. No space is therefore left unoccupied, as may be seen in Scheme 4b. In other words, it is assumed that the surface of the MWCNT is divided into a lattice of sites, each of which could accommodate exactly one nanoparticle.

The coverage of TOAB-stabilized gold nanoparticles at the surface of the alkyl-modified MWCNTs may be defined as a ratio of the nanotube surface area occupied by the nanoparticles (A_{occ}) to the total surface area accessible for the nanoparticles (A_{total}). Considering, however, the previous assumption that the MWCNT surface is divided into a lattice of sites, each the size of one nanoparticle, $A_{particle}$, the coverage may be described by eq 11.

$$cov_{th} = \frac{A_{occ}}{A_{total}} = \frac{n_{occ}A_{particle}}{n_{max}A_{particle}} = \frac{n_{occ}}{n_{max}} = \frac{n_{occ}}{n_{occ} + n_{vac}} \quad (11)$$

Here, n_{max} is the maximum number of accessible sites, n_{occ} is the number of occupied sites, and n_{vac} is the number of vacant sites.

It is further assumed that the nanoparticle occupying a site on the nanotube surface is in a bound state, while the vacant site is equivalent to the particle being in a nonbound state (Scheme 4c). The particle in the latter state can freely leave the vicinity of the nanotube and be replaced by another nanoparticle from the solution. This exchange process is assumed to be a stationary one, and the rate of particles leaving the vicinity of the nanotube ($r_{leaving}$) is equal to the rate of nanoparticles approaching the nanotube ($r_{approaching}$) ($r_{leaving} = r_{approaching}$, i.e., equilibrium conditions). It is further assumed that the exchange process is not limited by the diffusion of the nanoparticles in the solution. In other words, the number of particles in a nonbound state depends only on the interaction with the nanotube. Effectively, such assumptions enable the adsorption of the nanoparticles at the surface of a nanotube to be treated as a set of independent two-state processes.

Given the association between the occupied/vacant sites and bound/nonbound states of the nanoparticles, the coverage may be now defined as the probability (p) of a particle being in a bound state (which is also a number probability of a site being occupied, cf. eq 11).

SCHEME 4: (a) Illustration of the Theoretical Close Packing of Nanoparticles at the Surface of the MWCNTs, Representing a Maximum Possible Coverage (100%); (b) Illustration of Nanoparticles at the Surface of a MWCNT in a less than Optimum Configuration; (c) Illustration of Gold Nanoparticles at the Surface of a MWCNT in the Bound and Unbound States; (d) Representation of the Energy Well Describing the Interaction of a Nanoparticle at the Surface of a MWCNT as a Function of Distance

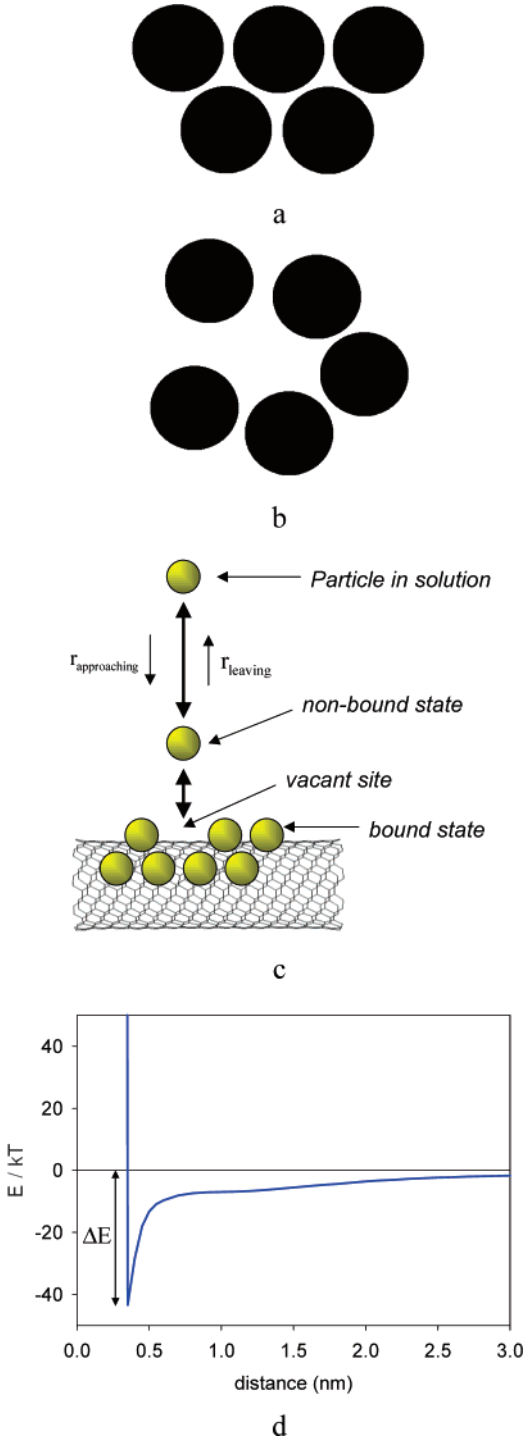

The attractive forces in the proximity of a nanotube may form a potential well of depth ΔE, as shown in Scheme 4d. Hence, the probability (p) may be defined as 1 minus the probability of overcoming that energy barrier, that is, jumping out of that energy well. The latter depends also on a number of unknown factors such as the dynamics of the local environment including fluctuations in the ligand chain densities, interaction with other nanoparticles in the solution, and behavior of the system during drying of the drop of the solution on the TEM grid. To account for these phenomena in the simplest possible manner, a modified Boltzmann-type energy distribution has been taken. Therefore, the theoretical coverage has been defined as eq 12:

$$\mathrm{cov_{th}} = \left(1 - \exp\left(-\frac{\Delta E}{\alpha kT}\right)\right)\cdot 100\% \qquad (12)$$

The scaling parameter (α) is introduced to account for the above-mentioned dynamical and local phenomena.

Experimental Section

Materials. All solvents and compounds were used as supplied by the Sigma-Aldrich Chemical Co. Ltd., unless otherwise stated. The MWCNTs used in this study were supplied by MER Corporation. The MWCNTs were the "as-produced cathode deposit" during the Kratschmer−Huffman arc process. Deionized−distilled Millipore MilliQ water was used for all washing steps and in reactions carried out in water.

Characterization Techniques. All TEM images were obtained using a JEOL 2000 FX TEMscan instrument (at an accelerating voltage of 80 kV) for samples deposited on both uncoated (2000 mesh) and carbon-coated (400 mesh) copper grids. The preparation of samples for TEM analysis involved depositing a drop (20 μL) of the relevant dispersion or suspension onto one of the above grids.

All Fourier transform infrared (FT-IR) spectra were obtained using a Matteson Galaxy FT-IR spectrometer. Spectra of solids (including MWCNTs) were obtained using KBr pellets (0.05 mg in 100.00 mg of KBr), while spectra of liquids were obtained using a CaF_2 solution cell (Specac, Omni-Cell, 50 μm path length).

^{1}H NMR spectra were recorded using either Varian 300 MHz FT-NMR or Varian 500 MHz FT-NMR spectrometers with either the solvent or tetramethylsilane (TMS) as the reference. All chemical shifts are quoted on the δ scale. All coupling constants are expressed in hertz. Suspensions, dispersions, and solutions used in the above ^{1}H NMR spectroscopic studies were prepared from dry samples of the desired MWCNT, nanoparticle, or compound by addition of the appropriate deuterated solvent.

UV−visible spectroscopy experiments were performed using a HP-8452A spectrophotometer and LabView software written to acquire data. All UV−visible spectra were referenced using appropriate solution backgrounds.

Preparation of Purified Unmodified MWCNTs. As-received MWCNTs were purified from graphitic impurities using a recently reported methodology involving the sequential sonication and centrifugation of the MWCNTs in solution.[19]

Preparation of Carboxy-Modified MWCNTs. MWCNTs were modified in order to introduce carboxy groups at the surface of the nanotubes.[51,52] The MWCNTs were refluxed in nitric acid in order to produce hydroxyl, carbonyl, and carboxy groups at defects in the carbon atom lattice. The above hydroxyl and carbonyl groups were further oxidized to carboxy groups by treatment with potassium permanganate and perchloric acid. A detailed experimental methodology has recently been reported.[19]

Preparation of Acid Chloride-Modified MWCNTs. Carboxy-modified MWCNTs (3 mg) were suspended by sonication in $SOCl_2$ (15 mL, 0.20 mol) and heated to 70 °C for 24 h under magnetic stirring. The unreacted $SOCl_2$ and the SO_2 and HCl

byproducts were removed by rotary evaporation under reduced pressure, followed by drying using a Schlenk apparatus for 6 h.

Preparation of Propylamine-Modified MWCNTs (PA-MWCNTs) involved the formation of an amide between acid chloride-modified MWCNTs and propylamine. A detailed experimental methodology has recently been reported.[20]

Preparation of Pentylamine-Modified MWCNTs (PTA-MWCNTs) and Octylamine-Modified MWCNTs (OA-MWCNTs) involved the formation of an amide between acid chloride-modified MWCNTs and PTA/OA.

Pentylamine (PTA) (10 mL, 8.63×10^{-2} mol) or octylamine (OA) (10 mL, 6.40×10^{-2} mol) was added to dry acid chloride-modified MWCNTs (3 mg) and the material sonicated for 15 min to ensure complete dispersion of the MWCNTs. The suspension was stirred for 12 h, with sonication for 5 min at 1 h intervals. The PTA-modified MWCNTs and OA-modified MWCNTs were filtered through an alumina filter membrane (Anodisc, Whatman-UK 0.2 μm pore diameter) and washed with ethanol (200 mL). The PTA-modified MWCNTs and OA-modified MWCNTs were sonicated off the filter membrane into ethanol (200 mL) and sonicated for 15 min to ensure any residual unreacted PTA or OA was dispersed. The suspensions of PTA-modified MWCNTs and OA-modified MWCNTs were filtered through an alumina filter membrane (Anodisc, Whatman-UK 0.2 μm pore diameter) and washed with ethanol (200 mL), followed by chloroform (200 mL). The PTA-modified MWCNTs and OA-modified MWCNTs were sonicated off the filter membrane into ethanol (10 mL). The ethanol was removed by rotary evaporation, followed by drying using a Schlenk apparatus (2 h). The dry PTA-modified MWCNTs and OA-modified MWCNTs were dispersed in chloroform (10 mL) by sonication (10 min).

Preparation of Dodecylamine-Modified MWCNTs (DDA-MWCNTs) involved the formation of an amide between acid chloride-modified MWCNTs and DDA.

Dodecylamine (DDA) (10 g, 5.40×10^{-2} mol) was added to dry acid chloride-modified MWCNTs (3 mg) and heated to 30 °C. The mixture was sonicated for 15 min to ensure complete dispersion of the MWCNTs. The suspension was stirred for 12 h, with sonication for 5 min at 1 h intervals. The DDA-modified MWCNTs were filtered through an alumina filter membrane (Anodisc, Whatman-UK 0.2 μm pore diameter) and washed with ethanol (200 mL). The DDA-modified MWCNTs were sonicated off the filter membrane into ethanol (200 mL) and sonicated for 15 min to ensure any residual unreacted DDA was dispersed. The suspension of DDA-modified MWCNTs was filtered through an alumina filter membrane (Anodisc, Whatman-UK 0.2 μm pore diameter) and washed with ethanol (200 mL), followed by chloroform (200 mL). The DDA-modified MWCNTs were sonicated off the filter membrane into ethanol (10 mL). The ethanol was removed by rotary evaporation, followed by drying using a Schlenk apparatus (2 h). The dry DDA-modified MWCNTs were dispersed in chloroform (10 mL) by sonication (10 min).

Preparation of Mercaptoethylamine-Modified MWCNTs (MEA-MWCNTs) involved the formation of an amide between acid chloride-modified MWCNTs and MEA.

A solution of 2-mercaptoethylamine hydrochloride (50 mg, 4.40×10^{-4} mol) in pyridine (10 mL, 0.12 mol) was added to dry acid chloride-modified MWCNTs (3 mg) and the mixture sonicated (15 min) to ensure complete dispersion of the MWCNTs. The suspension was heated to 40 °C and allowed to stir for 12 h, with intermittent sonication for 5 min at 1 h intervals. The dispersion was filtered using an alumina filter membrane (Anodisc, Whatman-UK 0.2 μm pore diameter) and washed with ethanol (200 mL). The MEA-modified MWCNTs were sonicated off the filter membrane into ethanol (200 mL) and sonicated for 15 min to ensure any residual unreacted MEA was dispersed. The suspension of MEA-modified MWCNTs was filtered through an alumina filter membrane (Anodisc, Whatman-UK 0.2 μm pore diameter) and washed with ethanol (200 mL), followed by chloroform (200 mL). The MEA-modified MWCNTs were sonicated off the filter membrane into ethanol (10 mL). The ethanol was removed by rotary evaporation, followed by drying using a Schlenk apparatus (2 h). The dry MEA-modified MWCNTs were dispersed in chloroform (10 mL) by sonication (10 min).

Preparation of Mercaptohexanol-Modified MWCNTs (MHO-MWCNTs) and Mercaptoundecanol-Modified MWCNTs (MUDO-MWCNTs) involved the formation of an ester between acid chloride-modified MWCNTs and MHO or MUDO.

A solution of 6-mercapto-1-hexanol (6.0×10^{-2} mL, 4.40×10^{-4} mol) or 11-mercapto-1-undecanol (90 mg, 4.40×10^{-4} mol) in pyridine (10 mL, 0.12 mol) was added to dry acid chloride-modified MWCNTs (3 mg) and the material sonicated (15 min) to ensure complete dispersion of the MWCNTs. The dispersions were filtered using an alumina filter membrane (Anodisc, Whatman-UK 0.2 μm pore diameter) and washed with ethanol (200 mL). The MHO-modified MWCNTs or MUDO-modified MWCNTs were sonicated off the filter membrane into ethanol (200 mL) and sonicated for 15 min to ensure any residual unreacted MHO or MUDO was dispersed. The dispersions of MHO-modified MWCNTs and MUDO-modified MWCNTs were then filtered through an alumina filter membrane (Anodisc, Whatman-UK 0.2 μm pore diameter) and washed with ethanol (200 mL), followed by chloroform (200 mL). The MHO-modified MWCNTs and MUDO-modified MWCNTs were sonicated off the filter membrane into ethanol (10 mL). The ethanol was removed by rotary evaporation, followed by drying using a Schlenk apparatus (2 h). The dry MHO-modified MWCNTs and MUDO-modified MWCNTs were dispersed in chloroform (10 mL) by sonication (10 min).

Preparation of Tetraoctylammonium Bromide (TOAB)-Stabilized Gold Nanoparticles. Tetraoctylammonium bromide (TOAB)-stabilized gold nanoparticles were synthesized using a modification of the two-phase synthesis originally described by Fink et al.[35] Briefly, tetraoctylammonium bromide (1.00 g, 1.80 mmol) in chloroform (50 mL) was combined with an aqueous solution of hydrogen tetrachloroaurate (35.5×10^{-3} g, 0.09 mmol, 3 mL) and the resulting orange solution vigorously stirred for 30 min. The aqueous phase was discarded, and to the stirred organic phase an aqueous solution of sodium borohydride (37.80×10^{-3} g, 1.00 mmol, 2.5 mL) was added dropwise (20 μL) at a rate of one drop every 15 s, until the color of the solution had changed from orange to yellow to clear. At this point, the remainder of the sodium borohydride solution was added, upon which the color of the solution turned deep purple. The resulting nanoparticle dispersion was stirred for 6 h, after which the aqueous phase was separated and the remaining organic phase dried over magnesium sulfate.

Preparation of Dodecanethiol (DDT)-Stabilized Gold Nanoparticles. Dodecanethiol-stabilized gold nanoparticles were synthesized using a procedure similar to the two-phase synthesis procedure originally described by Brust et al.[53] Briefly, tetraoctylammonium bromide (1.051 g, 1.92 mmol) in chloroform (32 mL) was combined with an aqueous solution of

hydrogen tetrachloroaurate (0.154 g, 0.40 mmol, 10 mL) and the resulting orange solution vigorously stirred for 30 min. The aqueous phase was discarded, and an aqueous solution of sodium borohydride (0.120 g, 3.20 mmol, 10 mL) was added dropwise (20 μL) to the stirred organic phase. This was followed after 30 s by the addition of dodecanethiol (0.186 mL, 0.80 mmol). The resulting nanoparticle dispersion was stirred for 6 h, after which the volume of the solution was reduced to 3 mL using rotary evaporation. The nanoparticle dispersion was then precipitated by the addition of ethanol (20 mL), and the precipitated nanoparticles recovered by centrifugation. The nanoparticle precipitate was allowed to dry in air and was finally dispersed in chloroform (10 mL).

Templated Assembly of Nanoparticles at the Surface of Unmodified and Modified MWCNTs. The experimental conditions used for the combination of gold nanoparticles and unmodified and modified MWCNTs in solution were similar in all cases.

Templated Assembly of TOAB-Stabilized Gold Nanoparticles at the Surface of Unmodified and Modified MWCNTs. MWCNTs (0.2 mL, 3×10^{-4} g mL^{-1}) were added to chloroform (0.8 mL) and sonicated for 3 min. TOAB-stabilized gold nanoparticles (0.030 mL, 1.40×10^{15} nanoparticles/mL) were added to the dispersion and the mixture allowed to equilibrate for 6 h. The mixture was sampled for TEM analysis by evaporation of a drop (20 μL) of the mixture onto a carbon-coated copper TEM grid.

Effect of the Addition of Dodecanethiol to the Templated Assembly of TOAB-Stabilized Gold Nanoparticles at the Surface of Unmodified and Modified MWCNTs. An excess of dodecanethiol was added to dispersions of TOAB-stabilized gold nanoparticles and MWCNTs following equilibration. The excess used was based on the total surface area of the gold nanoparticles in solution that would be susceptible to adsorption of the dodecanethiol molecules. The amount used was based on a mean particle diameter of 4.60 nm and the area occupied by a dodecanethiol molecule being 15.4 Å^2. MWCNTs (0.2 mL, 3×10^{-4} g mL^{-1}) were added to chloroform (0.8 mL) and sonicated for 3 min. TOAB-stabilized gold nanoparticles (0.030 mL, 1.40×10^{15} nanoparticles/mL) were added to the dispersion and the mixture allowed to equilibrate for 6 h. Dodecanethiol (1 μL, 4.2×10^{-6} mol) was added to the mixture and allowed to equilibrate for 6 h. The mixture was sampled for TEM analysis by evaporation of a drop of the mixture onto a carbon-coated copper TEM grid.

Control I: Combination of Dodecanethiol-Stabilized Gold Nanoparticles with Unmodified and Modified MWCNTs in Solution. A set of control experiments involving the combination of unmodified, alkyl-modified, and alkylthiol-modified MWCNTs with dodecanethiol-stabilized gold nanoparticles were performed and are described in detail in Supporting Information section S7.

MWCNTs (0.2 mL, 3×10^{-4} g mL^{-1}) were added to chloroform (0.8 mL) and sonicated for 3 min. DDT-stabilized gold nanoparticles (0.026 mL, 1.63×10^{15} nanoparticles/mL) were added to the dispersion and the mixture allowed to equilibrate for 6 h. The mixture was then sampled for TEM analysis by evaporation of a drop (20 μL) of the mixture onto a carbon-coated copper TEM grid. Full details for this control experiment are described in Supporting Information section S7.

Characterization of MWCNT−Nanoparticle Systems. Following equilibration of MWCNT−nanoparticle samples, a drop of each sample was evaporated onto a carbon-coated copper TEM grid for analysis by TEM.

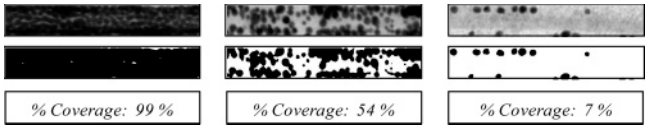

Figure 3. TEM images of gold nanoparticles assembled at the surface of 200 nm sections of MWCNTs and the corresponding threshold adjusted images used to calculate the percentage coverage.

Analysis of the TEM images using threshold analysis involved the selection of a 200 nm section of the MWCNTs. The threshold of a selected section was manually adjusted using conventional image processing software (Jasc Software, Paint Shop Pro, Version 7.00) so that the gold nanoparticles present in the image could be viewed in contrast with areas that contained no nanoparticles, in black and white, respectively. By this means, a ratio of the area occupied by gold nanoparticles to the area available at the surface of the nanotube was obtained and expressed as percentage coverage, as illustrated in Figure 3.

The experimental coverage obtained in this way represents a ratio of the visible area occupied by the nanoparticles (A^*_{occ}) to the total visible area of the nanotube (A^*_{total}). It is noted, however, that a TEM image presents a projection of the three-dimensional (cylindrical) surface of a MWCNT onto the plane of the image, which distorts the observed coverage especially near the edges of the visible side of the MWCNT. The procedure of reading the coverage from a TEM image treats the imaged objects as flat, ignoring the above effect. This could lead to inaccuracies, but the parts of the nanoparticles visible outside the outline of the nanotube are also ignored; therefore, the two effects should cancel out. Hence, the ratio A^*_{occ}/A^*_{total} should be a good representation of the real ratio of occupied nanotube surface (A_{occ}) to the total accessible area of the nanotube (A_{total}). Thus, if the nanoparticle arrangement assumptions are fulfilled, then the formulas for theoretical and experimental coverages are equivalent (cf. eq 12).

Results and Discussion

Preparation and Characterization of MWCNTs and TOAB-Stabilized Gold Nanoparticles. The synthesis of MWCNTs using the arc discharge technique is known to produce nanotubes in high yield in addition to significant amounts of graphitic impurities. In view of this, recent years have seen a large number of reports concerned with the purification of nanotube samples.[54] Many of these reports have described the purification of CNTs from graphitic impurities using both chemical and physical means. In the context of the work described here, a high-quality CNT starting material is a particular requirement for the assembly of nanoscale materials in solution. A further requirement is the ability to purify CNTs while maintaining the physical and chemical properties of the starting material. Therefore, an initial purification procedure consisting of multiple sonication and centrifugation steps was performed.

The purification procedure uses sonication as a means to disperse the MWCNTs in chloroform. At a low concentration of MWCNTs (1.50×10^{-4} g mL^{-1}), sonication for 15 min yields a dark suspension of the material in chloroform. Centrifugation of this suspension results in the precipitation of aggregated carbonaceous material, while the supernatant containing suspended MWCNTs is retained. This process is repeated several times until a transparent grey-brown MWCNT suspen-

sion is achieved. It is believed that the sonication of the MWCNT material allows the attractive van der Waals forces between MWCNTs and the amorphous carbon impurities to be overcome and results in the material being suspended in solution. Centrifugation of the suspension results in the, presumably denser, amorphous carbon impurities being precipitated from the suspension, leaving the less dense MWCNTs suspended in solution. TEM analysis of the suspension before and after the process proving the successful purification has been recently reported.[19,20] It is noted that the sonication of CNT samples has been reported to cause structural damage to CNTs.[55] No significant structural damage to the MWCNTs was observed in this work, even though MWCNTs were sonicated for 15 min on several occasions. The MWCNTs were of good quality and retained their structural integrity. TEM analysis of 50 individual MWCNTs showed the mean diameter to be 24 nm and the length to be in the range 1.5−2.0 μm.

Subsequently, the MWCNTs were modified in order to introduce carboxy groups at the surface of the nanotubes.[51,52] The MWCNTs were refluxed in nitric acid in order to produce hydroxyl, carbonyl, and carboxy groups in the carbon atom lattice. In particular, these groups may be localized at defects and dislocations in the carbon lattice and at sites which exhibit increased sp^3 character. The above hydroxyl and carbonyl groups were further oxidized to carboxy groups by treatment with potassium permanganate and perchloric acid.

Rao and co-workers have determined that the number of carboxy functional groups present in samples of MWCNTs following oxidative treatments to be of the order of 10^{21} sites/g.[56] This figure is also in agreement with the work reported by Hiura and co-workers who, in addition, have reported that the outer layer of typical MWCNTs constitutes approximately 15% of the total carbon present in the tubes.[57] Estimating that the oxidation occurs predominantly at the outer nanotube layer, it is calculated that approximately 13.3% of the surface carbon layer contains carboxy functional groups. On this basis, the number of functional groups present is of the order of 1 in every 7.5 carbon atoms. Taking the C═C bond length to be 1.42 Å, an area of 1 nm^2 is estimated to encompass an average of 41 carbon atoms in a planar graphene surface. This yields a value of 5.4 defect sites/nm^2. This figure serves as an approximation of the density of surface carboxy groups, which may be available for further functionalization using covalent chemistry.

The covalent modification of carboxylic acid groups at the surface of CNTs is well-known and has been used as a means to couple a diverse range of molecular and condensed phase materials to the surface of CNTs.[11,12] In general, this is achieved via diimide activated ester and amide formation or by the conversion of the acid to an acid chloride and the subsequent formation of esters and amides. The latter approach is used in the work described here, on account of the ease with which this method may be used to covalently couple a range of amine- and alcohol-terminated molecules. The molecules which were coupled to the surface of MWCNTs via ester and amide formation included the following: propylamine (PA), pentylamine (PTA), octylamine (OA), dodecylamine (DDA), mercaptoethylamine (MEA), mercaptohexanol (MHO), and mercaptoundecanol (MUDO).

As a result of the variation in the physical properties of the reagents used, several variations of a general synthetic procedure were employed. The general synthetic procedure may be schematically illustrated, as shown in Scheme 5.

TOAB-stabilized gold nanoparticles were prepared as described in detail in the Experimental Section and characterized

SCHEME 5: General Synthetic Procedure Used to Covalently Couple Alcohol- and Amine-Terminated Molecules to MWCNT-Bound Acid Chloride Groups

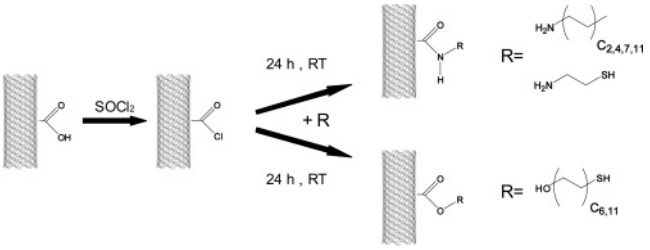

by TEM. The mean particle diameter was found to be 4.60 nm with a polydispersity of 1.08, on the basis of the analysis of 200 particles (see Supporting Information section S9).

MWCNTs have been covalently modified with a series of alkyl chains of increasing lengths and combined with TOAB-stabilized gold nanoparticles in solution, as described earlier. It was anticipated that varying the alkyl chain length would provide an effective means of controlling the distance of separation between the TOAB-stabilized gold nanoparticles and the surface of the MWCNTs and, furthermore, would enable key assumptions and predictions of the theoretical model to be experimentally validated.

Noncovalent Case. The templated assembly of TOAB-stabilized gold nanoparticles at the surface of unmodified and alkyl-modified MWCNTs was observed following the addition of an aliquot of a gold nanoparticle dispersion to a dispersion of MWCNTs. After equilibration (24 h), a drop of the suspension was sampled for analysis by TEM. TEM was used to image the nanoparticles adsorbed at the surface of the MWCNTs. A subsequent analysis of the TEM images was used to quantify the extent of nanoparticle adsorption at the surface of the MWCNTs, thus giving an estimate of the percentage coverage of gold nanoparticles. Figure 4 shows the TEM images of unmodified and alkyl-modified MWCNTs following their combination with TOAB-stabilized gold nanoparticles.

There is a trend apparent in Figure 4; specifically, the coverage of gold nanoparticles at the surface of the MWCNTs decreases with increasing alkyl chain length. Full coverage was observed for unmodified and PA-modified (C_3) MWCNTs (the former finding is in agreement with that previously reported by Fullam et al.[18]). In the case of PTA-modified MWCNTs (C_5), the adsorption covered around half of the available surface. Significantly decreased coverage (5−10%) was observed for OA-modified (C_8), while very few particles, of the order of 1−2%, were adsorbed for the longest studied alkyl chains, that is, DDA-modified MWCNTs (C_{12}). All experimental results are summarized in Table 1.

To compare the theoretical predictions of the model presented in this paper with experimental findings, the total interaction energy between the alkyl-modified MWCNTs and TOAB-stabilized gold nanoparticles was calculated for alkyl chain lengths corresponding to experimental data from Table 1. The length of the chain (L_a) is taken as the distance between the carbonyl and terminal methyl group of the alkyl chain for respective *N*-(*n*-alkyl)acetamide as modeled by CS ChemDraw3D software: 0 nm (C_0), 0.500 nm (C_3), 0.752 nm (C_5), 1.137 nm (C_8), and 1.644 nm (C_{12}). The length of the TOAB chains (L_T) was taken as 1.200 nm (following the study of TOAB-stabilized gold nanoparticles by Fink et al.[35]), while the radii of MWCNTs and gold nanoparticles (12.0 and 2.3 nm, respectively) were taken as averages from the TEM images (see Supporting Information section S9). The alkyl chain volume fraction at the

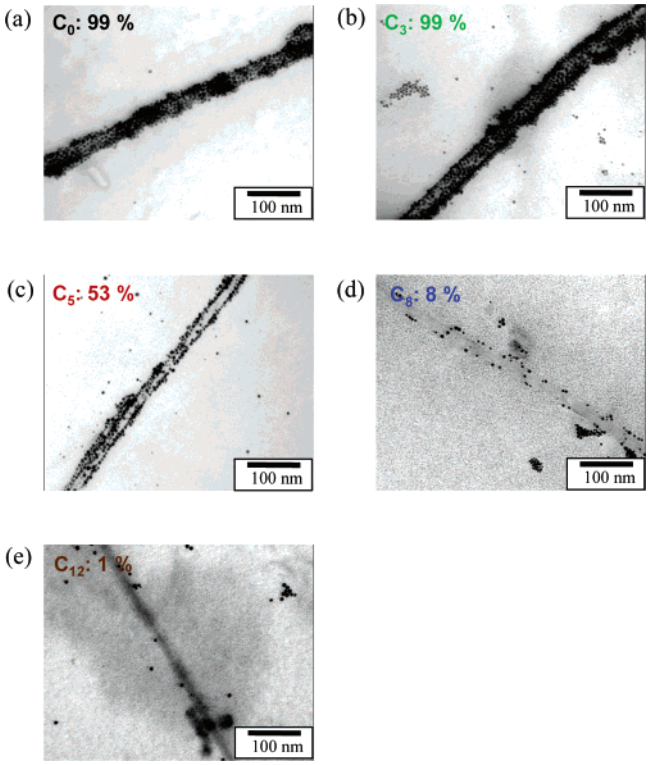

Figure 4. TEM images of (a) unmodified and (b−e) alkyl-modified MWCNTs (C_3, C_5, C_8, and C_{12}, respectively) following their combination with TOAB-stabilized gold nanoparticles.

TABLE 1: Coverage of TOAB-Stabilized Gold Nanoparticles at the Surface of Unmodified and Alkyl-Modified MWCNTs (See Supporting Information for Complete Analysis)

name	abbrev	tubes analyzed	average coverage (%)	standard deviation (%)
MWCNTs	C_0	17	97	3
PA-MWCNTs	C_3	8	96	3
PTA-MWCNTs	C_5	30	47	10
OA-MWCNTs	C_8	12	7	2
DDA-MWCNTs	C_{12}	12	2	2

surface of the MWCNT ($\phi_{CNT}(0)$) was calculated from the density of defects on the MWCNT to be equal 0.68. The nanoparticle−nanoparticle interaction model was used to calculate the volume fraction of TOAB chains at the surface of the gold nanoparticle,[28] $\phi_p(0) = 0.35$, on the basis of the reported separation between the TOAB-stabilized nanoparticles.[35] The resulting energy profiles, shown in Figure 5a, were used to calculate the energy wells (ΔE) in each case.

Using ΔE, the theoretical coverage of gold nanoparticles at the surface of the unmodified and alkyl-modified MWCNTs was determined according to eq 12, with the α parameter equal to 20. These results are compared in Figure 5b with the experimental results from Table 1.

The agreement between the theoretical and experimental results is gratifying, although there are some minor discrepancies for the longer chain systems, where the theoretical model appears to overestimate the coverage. This agreement provides important insights into the nature of the interactions between TOAB-stabilized gold nanoparticles and unmodified and modified MWCNTs, which are considered below.

For C_0−C_3 systems, the steric repulsion is either absent or too weak to prevent a nanoparticle from closely approaching the surface of the nanotube. For such systems, attractive forces dominate up to very short separations and are eventually limited

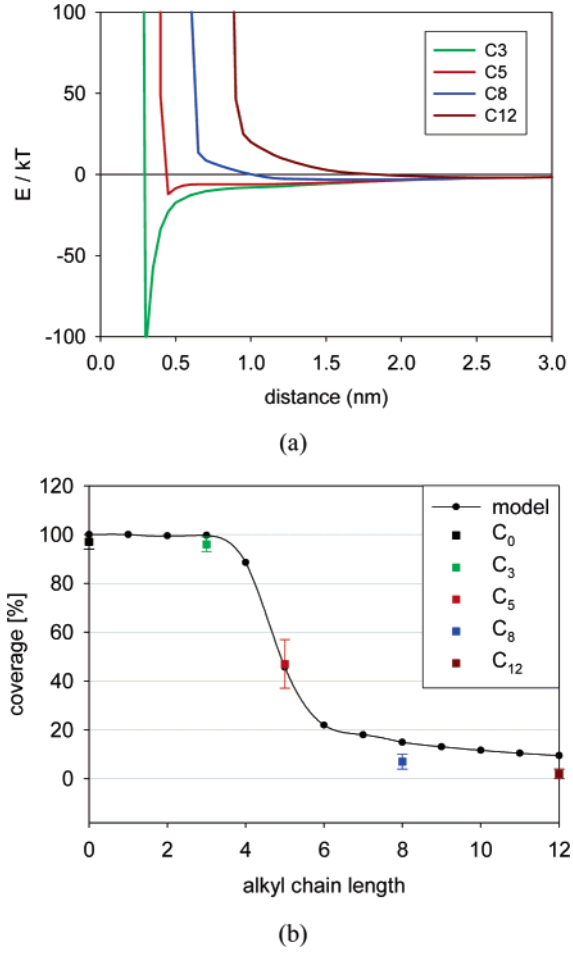

Figure 5. (a) Total noncovalent interactions for a range of alkyl chain lengths (C_3, C_5, C_8, and C_{12}). (b) Theoretical prediction and experimental results of the percentage coverage for TOAB-stabilized gold nanoparticles at the surface of unmodified and alkyl-modified MWCNTs as a function of alkyl chain length.

by nonelastic repulsion. Deep energy wells for such systems ensure relatively strong binding of the nanoparticles to the surface of the nanotube. It can be reasoned that the high degree of coverage observed in the C_0 case (99%) is a consequence of sterically unhindered adsorption of the gold nanoparticles at the surface of the MWCNTs, which is stabilized predominantly by the charge transfer interaction and also by van der Waals attractions. In the C_3 case, the high degree of coverage observed (99%) is due to the close approach of the gold nanoparticles to the PA-MWCNTs, which allows a charge transfer and van der Waals attractions to persist. This is despite the presence of a layer of short alkyl chains, which undoubtedly hinders to some extent the approach of the gold nanoparticles. It is noted that, in this case, the relative importance of the van der Waals attractive forces is thought to be greater than that of the C_0 system.

In contrast to the C_0−C_3 systems, the repulsive character dominates the interactions for systems from C_8−C_{12}, with a shallow potential energy minimum at distances of 1.2−2.0 nm due to the long-range character of the van der Waals forces and relatively weak osmotic repulsion. The low degree of coverage observed from the experimental results for the C_8 and C_{12} systems (8 and 1.5%, respectively), is concluded to be due to the sterically hindered approach of the gold nanoparticles to the surface of the MWCNTs on account of the layer of alkyl chains. As a result of this steric barrier, in these cases, attractive charge transfer and van der Waals interactions are insufficient

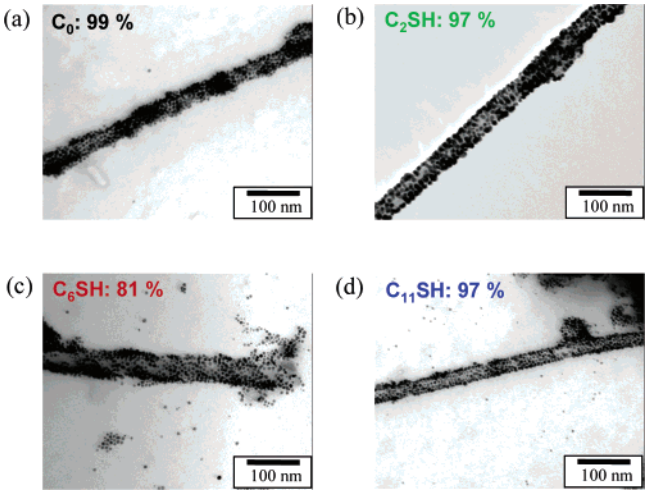

Figure 6. TEM images of alkylthiol-modified MWCNTs (MEA-(C_2SH), MHO- (C_6SH), and MUDO-MWNTs ($C_{11}SH$)) following their combination with TOAB-stabilized gold nanoparticles.

to provide the driving force for the adsorption of gold nanoparticles.

The C_5 system represents an intermediate case with an almost flat energy landscape for separations ranging from 0.6 to 1.5 nm and a weak energy well for $d \cong 0.5$ nm. From the experimental results, the average coverage of 47% confirms that this system is particularly sensitive and represents a transition between the domination of the attractive interactions in the C_0-C_3 systems and the domination of the repulsive interactions of the C_8-C_{12} systems. The standard deviation is significantly higher for the C_5 system (10%) than that for the C_0-C_3 and C_8-C_{12} systems (3 and 2%, respectively), which further supports the views expressed above. Therefore, the observed sensitivity of this system represents a potential opportunity for the development of materials which are highly sensitive to the local environment, whereby the modification of such a system by a methylene group would allow a transition between high coverage and low coverage of nanoparticle systems to be mediated. More specifically, these and related materials offer the prospect of nanoscale devices capable of displaying gain in the output signal, as will be discussed elsewhere.

Covalent Case. In the noncovalent case of alkyl-modified MWCNTs, it has been shown that the extent of nanoparticle adsorption is dependent on the length of the alkyl chains, which dictates the distance of separation between the nanoparticles and the nanotubes. However, in view of the reports of the modification of CNTs with thiol-terminated molecules as a means by which gold nanoparticles may be adsorbed at the surface of CNT templates,[52] it is expected that covalent gold−thiol bond formation will dominate the interaction between the gold nanoparticles and the alkylthiol-modified MWCNTs. Thus, it is important to test whether the alkyl chain length is also a controlling parameter for the covalent case.

By analogy with the noncovalent case, the templated assembly of TOAB-stabilized gold nanoparticles at the surface of alkylthiol-modified MWCNTs is observed following the addition of an aliquot of a gold nanoparticle dispersion to a dispersion of MWCNTs. Following equilibration (24 h), a drop of the suspension was sampled for analysis by TEM. TEM was used to image the nanoparticles adsorbed at the surface of the MWCNTs and subsequently to quantify the extent of the adsorption (see Figure 6).

It was found that gold nanoparticles had formed a monolayer at the surface of the alkylthiol-modified MWCNTs in all three cases of alkylthiol chain length. All experimental data corresponding to the covalent assembly are shown in Table 2.

TABLE 2: Coverage of TOAB-Stabilized Gold Nanoparticles at the Surface of Alkylthiol-Modified MWCNTs (See Supporting Information for Complete Analysis)

name	abbrev	tubes analyzed	average coverage (%)	standard deviation (%)
MEA-MWCNTs	C_2SH	12	97	2
MHO-MWCNTs	C_6SH	8	83	7
MUDO-MWCNTs	$C_{11}SH$	8	93	4

TABLE 3: Effect of the Addition of DDT on the Coverage of TOAB-Stabilized Gold Nanoparticles at the Surface of Unmodified and Alkyl-Modified MWCNTs (See Supporting Information for Complete Analysis)

name	abbrev	tubes analyzed	average coverage (%)	standard deviation (%)
MWCNTs	C_0	4	1	0.7
PA-MWCNTs	C_3	4	1	0.6
PTA-MWCNTs	C_5	4	1	0.2
OA-MWCNTs	C_8	4	1	0.3
DDA-MWCNTs	C_{12}	4	1	0.2

TABLE 4: Effect of the Addition of DDT on the Coverage of TOAB-Stabilized Gold Nanoparticles at the Surface of Alkylthiol-Modified MWCNTs (See Supporting Information for Complete Analysis)

name	abbrev	tubes analyzed	average coverage (%)	standard deviation (%)
MEA-MWCNTs	C_2SH	4	91	3.1
MHO-MWCNTs	C_6SH	4	1	0.7
MUDO-MWCNTs	$C_{11}SH$	4	1	1.1

By analogy with the noncovalent case, the total interaction energy profiles were calculated according to eq 8 for alkylthiol chain lengths corresponding to MEA, MHO, and MUDO modifications of the MWCNTs. The chains lengths were calculated using CS ChemDraw3D (distances between the carbonyl and sulfur atoms) as 0.521 nm (C_2SH), 1.018 nm (C_6SH), and 1.656 nm ($C_{11}SH$). The covalent energy per thiol−gold bond was taken as $E_{Au-S}^{bond} = -67.5kT$.[58] Other parameters had the same values as in the noncovalent case.

Using the calculated interaction potentials (see Figure 7a), the theoretical coverage of gold nanoparticles at the surface of the alkylthiol-modified MWCNTs was determined according to eq 12. It is noted that the scaling parameter (α) was taken on the basis of values fitted for the data for the noncovalent case, that is, α parameter equal to 20. The theoretical predictions are compared with experimental data in Figure 7b, which show good agreement. It is clear from Figure 7a that the covalent term dominates the interaction, which is seen from the deep energy wells that exist at the distance of the alkylthiol chain lengths and similar shape of the energy profiles. It is particularly evident when compared with the depth of the interaction energy wells for the noncovalent case (Figure 5a), which are at least an order of magnitude shallower than the covalent case. Thus, the model predicts full coverage regardless of the chain length, as the osmotic and elastic repulsive terms are much weaker than the attractive covalent term.

Even though in the case of MEA-MWCNTs the gold−thiol bond formation was the dominant driving force for the adsorption of gold nanoparticles, it is also expected that, in view of the short chain length of the MEA ligands (C_2SH), charge transfer and van der Waals interactions may also both contribute. For longer chains (C_6SH, $C_{11}SH$), these noncovalent contributions are significantly smaller. It is also worth noting the

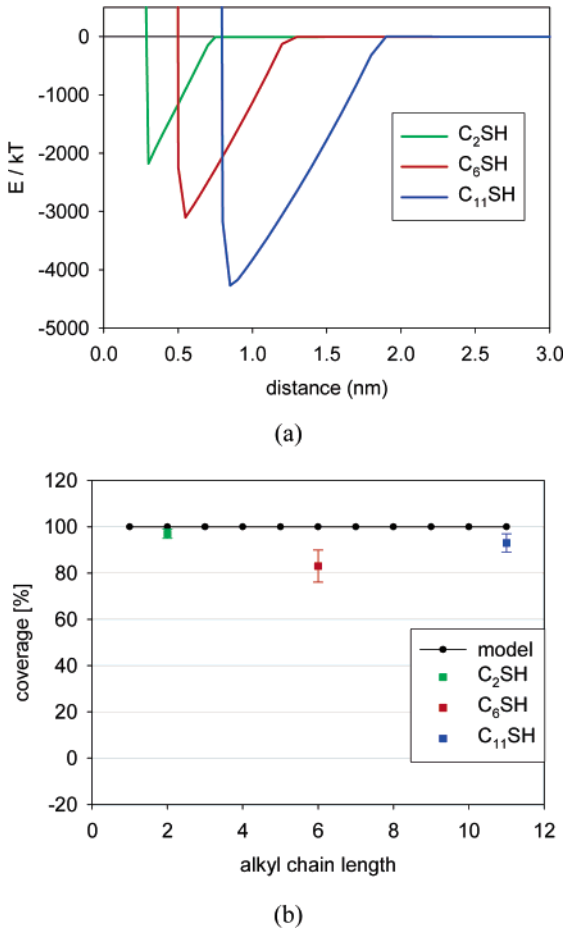

Figure 7. (a) Total covalent interactions for a range of alkylthiols (C_2SH, C_6SH, and $C_{11}SH$). (b) Theoretical prediction and experimental results of the percentage coverage for TOAB-stabilized gold nanoparticles at the surface of alkylthiol-modified MWCNTs.

difference in coverage between the noncovalent and covalent case for long alkyl chains, C_{12} and $C_{11}SH$. In the covalent case, a steric barrier does not need to be overcome to such extent as for the noncovalent case, because the thiol groups are at the ends of the alkylthiol chains. Thus, the covalent gold−thiol bonds can be formed even at separations corresponding to fully extended alkylthiol chains.

It is noted, however, that, in the C_6SH case, the experimental results are slightly lower than the predicted theoretical results. The reason for this difference may be the lateral mobility assumptions made when deriving the formula for the theoretical coverage. For very short chain lengths, there is no steric barrier for lateral motion of the nanoparticles on the surface of the nanotubes. Similarly, long chains have sufficient flexibility to allow the particle to "roll" on the surface. In both cases, the motion is not inhibited and the particles can achieve the best close packing possible. On the other hand, the intermediate length thiols, such as C_6SH, may provide a significant barrier to the "sliding" motion and have not enough flexibility for the "rolling" motion. Hence, a lower coverage may be expected.

Effect of Dodecanethiol for the Noncovalent Case. TOAB molecules have a relatively weak affinity for gold nanoparticles and can be easily replaced as the stabilizing ligand by ligands of higher affinity.[26,48] In this context, it is known that the surface of TOAB-stabilized gold nanoparticles may be readily modified by the adsorption of thiol molecules[59] and also that thiols adsorbed at the surface of gold nanoparticles may be displaced by other thiol molecules.[26] Therefore, it is expected that the addition of dodecanethiol (DDT) to TOAB-stabilized gold nanoparticles adsorbed at the surface of unmodified and alkyl-modified MWCNTs would result in the adsorption of the DDT ligands at the surface of the gold nanoparticles and the subsequent desorption of the gold nanoparticles from the MWCNTs.

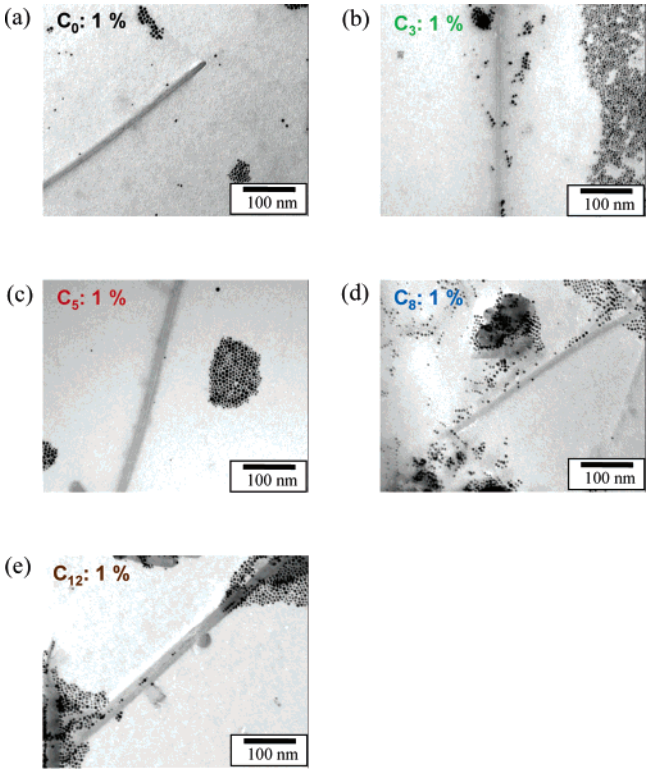

Figure 8. TEM images of (a) unmodified and (b−e) alkyl-modified MWCNTs (C_3, C_5, C_8, and C_{12}) following their combination with TOAB-stabilized gold nanoparticles and the subsequent addition of DDT.

Hence, following the combination of TOAB-stabilized gold nanoparticles and MWCNTs in solution, an excess of DDT was added to the materials which were allowed to equilibrate for 6 h. TEM was used to characterize the materials, and an analysis of the TEM images was performed to quantify the percentage coverage of gold nanoparticles at the surface of the MWCNTs, as shown in Figure 8.

Figure 8 shows that, as expected, the addition of DDT to unmodified and alkyl-modified MWCNTs following their combination with TOAB-stabilized gold nanoparticles resulted in desorption of the latter. Therefore, no coverage was observed (see Table 3). Theoretical explanation of this observation within the framework of the model is relatively simple. In the first stage, it involves estimating the energy gain due to the formation of multiple gold−thiol bonds and a change in the steric barrier due to replacing the TOAB with DDT as the stabilizing ligands. Considering that the nanoparticle before the addition of the DDT is likely to be located at the distance (d_0) corresponding to the well in the interaction energy profile, the potential of the nanoparticle may be expressed as

$$E^*(d) = E_{cov-CNT}(d_0) + E_{vdW}(d_0) + E_{CT}(d_0) + E_{st}(d_0) - E_{cov-DDT}(d_0) - E_{vdW}(d) - E_{CT}(d) - E_{osm-DDT}(d) - E_{elas-DDT}(d) \quad (13)$$

Here, $E_{st}(d_0) = E_{osm}(d_0) + E_{elas}(d_0) + E_{nonelas}(d_0)$, that is, a total steric energy at d_0, while $E_{cov-CNT}(d_0) = 0$ (the TOAB-stabilized

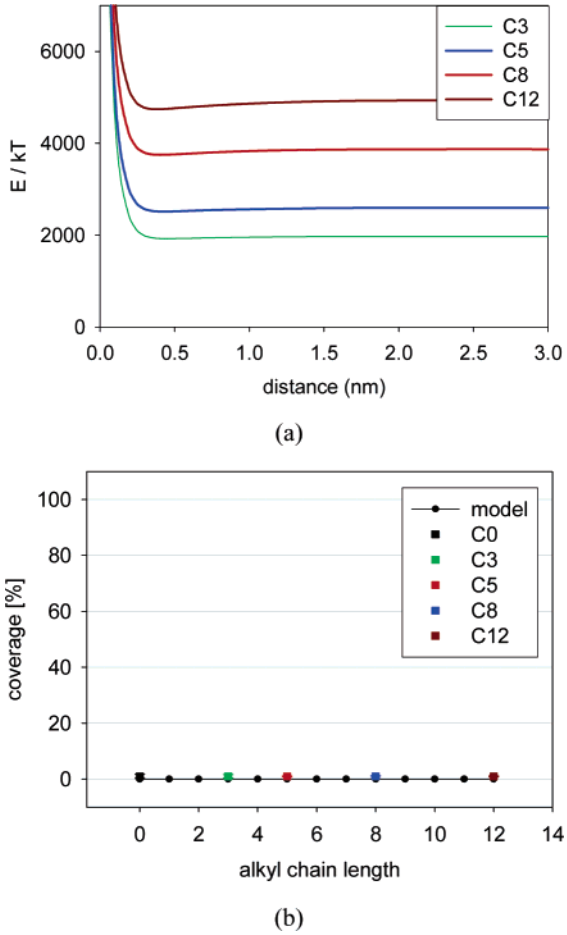

Figure 9. (a) Total potential energy profile of TOAB-stabilized gold nanoparticles at the surface of alkyl-modified MWCNTs (C_3, C_7, and C_{12}) in the presence of DDT. (b) Comparison of the theoretical prediction and experimental values of the percentage coverage of gold nanoparticles at the surface of alkyl-modified MWCNTs following the addition of DDT.

particles are not covalently bound to the nanotube). $E_{cov-DDT}(d)$ is the energy of gold−thiol bonds formed on the surface A_p of the nanoparticle which was shielded by the alkyl chains originating from the nanotube before the desorption (cf. Scheme 3 and Supporting Information section S4):

$$E_{cov-DDT}(d) = A_p(d)\rho_{thiols}E^{bond}_{Au-S} \qquad (14)$$

where $\rho_{thiols} = 6.25\ nm^{-2}$ is the density of thiols on gold[24] and E^{bond}_{Au-S} is given by eq 10. A positive value of the stability potential in eq 13 means the particle is unstable in the adsorbed state when subjected to the addition of DDT and desorbs. Figure 9a shows that this indeed is the case, due to the dominant effect of the formation of multiple gold−thiol bonds ($E_{cov-DDT}(d)$ has a negative sign in eq 14).

The potential energy well (ΔE) may be identified in this case as min $E^*(d)$ if $E^*(d) < 0$ for $d > 0$, that is, an effective barrier for desorption. Applying eq 12 leads to the coverage predictions shown in Figure 9b. Since $E^*(d) > 0$ irrespective of the alkyl chain length, the desorption is always favored and no coverage is predicted in all cases.

The second stage involves the analysis of the interaction between DDT-stabilized gold nanoparticles and alkylthiol-modified MWCNTs. This step is important in order to determine whether the DDT-stabilized gold nanoparticles can reassemble at the surface of the modified MWCNTs. Such a phenomenon would obviously influence the TEM observations. The procedure was analogous to the case of TOAB-stabilized gold nanoparticles, with the exception of a difference for nonelastic repulsion. The DDT molecules are not labile at the surface of the gold nanoparticles; therefore, the chains on both surfaces must be considered to prevent the volume fraction (ϕ) exceeding 1. The volume fraction of DDT molecules at the surface of the gold nanoparticle was taken as 0.79 (roughly scaling the coverage by thiols at the nanotube by $\rho_{thiols}/\rho_{COOH}$). The energy profiles for the interaction between DDT-stabilized gold nanoparticles and alkylthiol-modified MWCNTs are shown in Figure 10.

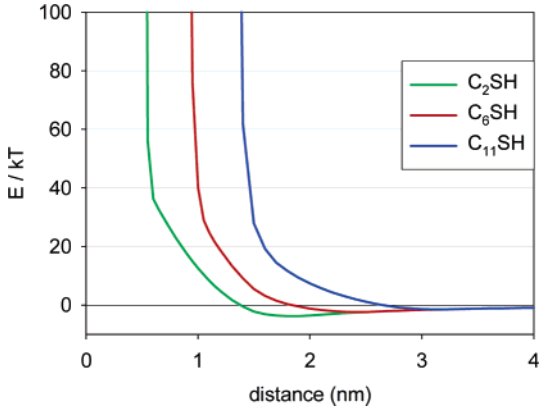

Figure 10. Energy profile of the interaction energy between DDT-stabilized gold nanoparticles and alkylthiol-modified MWCNTs.

It is evident that the interactions are predominantly repulsive, regardless of the chain length (C_2SH, C_6SH, $C_{11}SH$). The shallow minima observed at large separations between the nanoparticles and the MWCNTs are attributed to van der Waals attractive forces. This represents the steric barrier created by the presence of DDT at the surface of the nanoparticles. This suggests that, following the substitution of the TOAB molecules at the surface of the nanoparticles by DDT, the nanoparticles are repelled from the surface of the MWCNTs and are unlikely to come into close contact with the surface of the MWCNTs again.

This prediction is in full agreement with the control experiment involving the combination of DDT-stabilized gold nanoparticles with the full range of unmodified, alkyl-modified, and alkylthiol-modified MWCNTs, as described in detail in Supporting Information sections S7 and S10. In all of these cases, no adsorption of the DDT-stabilized gold nanoparticles at the surface of the MWCNTs was observed.

Effect of Dodecanethiol for the Covalent Case. The addition of DDT to TOAB-stabilized gold nanoparticles, which are adsorbed at the surface of alkylthiol-modified MWCNTs, provides a more interesting means of testing the predictive capability of the model. In this case, the nanoparticle is strongly bound to the nanotube, so the two strong interactions via gold−thiol bonds (MWCNT−nanoparticle and DDT−nanoparticle) effectively compete.

Hence, the alkylthiol-modified MWCNTs (MEA-, MHO-, and MUDO-MWCNTs) were combined with TOAB-stabilized gold nanoparticles in solution, and afterward, an excess of DDT was added to the materials, which were allowed to equilibrate for 6 h. An analysis of the corresponding TEM and threshold analysis were used to characterize the materials and quantify the percentage coverage (see Figure 11).

Interestingly, it was found that, in the case of the MEA-MWCNTs (C_2SH), gold nanoparticles remained at the surface of the MWCNTs (Figure 11b). On the other hand, in the case of MHO- and MUDO-MWCNTs (C_6SH and $C_{11}SH$), virtually

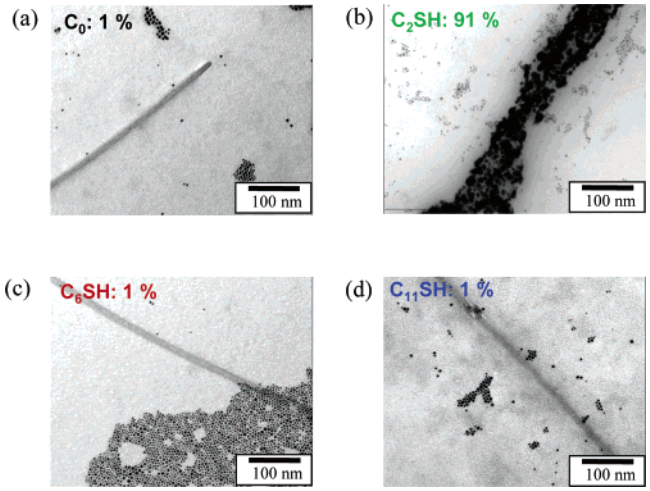

Figure 11. TEM image of (a) MEA-MWCNTs (C_2SH), (b) MHO-MWCNTs (C_6SH), and (c) MUDO-MWCNTs ($C_{11}SH$) following their combination with TOAB-stabilized gold nanoparticles and the subsequent addition of DDT.

no gold nanoparticles were observed at the surface of the MWCNTs (Figure 11c,d). Clearly, the experimental results indicate that the balance between these two interactions changes between short and long alkylthiol chains (see Table 4).

The covalent energy of binding the nanoparticle with the nanotube-bound alkylthiols was calculated according to eqs 9 and 10. These bonds have to be cleaved in case of desorption; thus, this energy constitutes the term $E_{cov-CNT}(d_0)$ in the current analysis (cf. eq 13). $E_{cov-CNT}(d)$ is calculated according to eq 14. Both binding energies are plotted and compared in Supporting Information section S5. It is noted that the energy of binding DDT to the surface of nanoparticles bound to the surface of an alkylthiol-modified MWCNT is always greater than the energy between the MWCNT-bound thiols and the gold nanoparticles. This is due to the higher possible density of thiol headgroups at the surface of the gold nanoparticles in comparison with the density of alkylthiol groups bound to the surface of the MWCNTs (the latter is due to the density of carboxyl groups at the surface). Therefore, the energy balance of bond cleavage (gold nanoparticles covalently adsorbed at the surface of alkylthiol-modified MWCNTs) and bond formation (DDT adsorbed at the surface of gold nanoparticles) suggests that the substitution by DDT is favored in all cases, irrespective of the alkylthiol chain length. Effectively, the bond energy changes considered separately are unable to account for the experimental results. In view of this, the steric effects must also be taken into consideration and the full form of the stability potential (eq 13) has to be calculated.

It is worth noting that a comparison of the steric potential energies for TOAB- and DDT-stabilized gold nanoparticles, that is, before and following the potential substitution with DDT, clearly shows the increase in steric repulsion and a shift of the nonelastic limit toward larger separations (see Supporting Information section S6). Hence, the substitution can only occur if accompanied by an increase in separation between the materials.

The stability potential energy of the TOAB-stabilized gold nanoparticles in the presence of DDT, shown in Figure 12a, shows that for mid-sized and longer chain lengths the substitution is favorable (stability potential $E^*(d) > 0$), but the substitution for very short chains at small separations needs to overcome an energy barrier of approximately $36kT$. An energy barrier of this size corresponds to a coverage of 84.5%, according to the calculations of the theoretical model based on

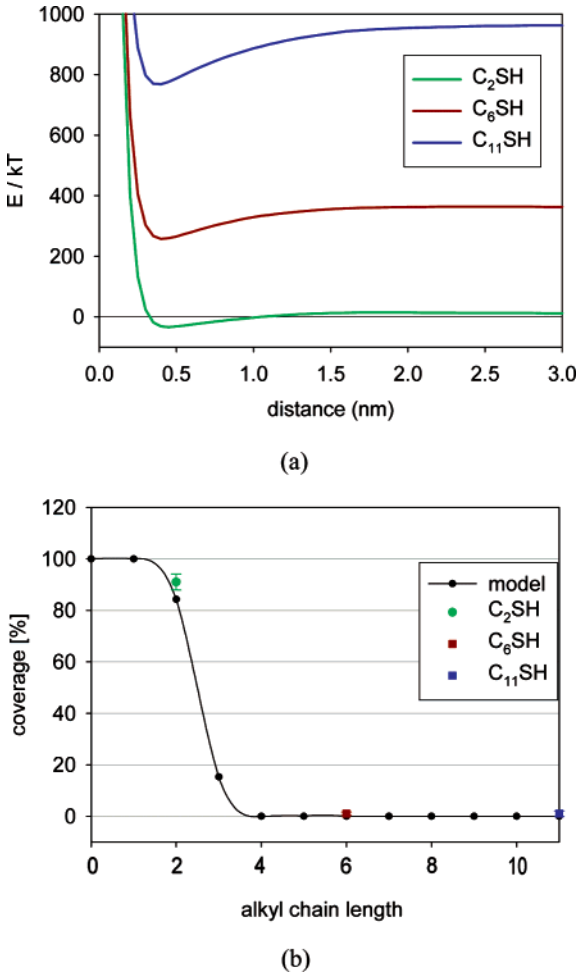

Figure 12. (a) Total potential energy profile of TOAB-stabilized gold nanoparticles at the surface of alkylthiol-modified MWCNTs (MEA-, MHO-, and MUDO-MWCNTs) in the presence of DDT. (b) Comparison of the theoretical prediction and experimental values of the percentage coverage of gold nanoparticles at the surface of alkylthiol-modified MWCNTs following the addition of DDT.

eq 12, with the same value of the $\alpha = 20$ parameter as previously used (this provides an independent test of the value obtained from the theoretical model). This is in good agreement with the experimental results obtained for the addition of DDT to TOAB-stabilized gold nanoparticles adsorbed at the surface of MEA-modified MWCNTs, as shown in Figure 11a. The attractive interactions experienced at short alkylthiol chain lengths, such as charge transfer and van der Waals forces, supplement the covalent interactions and as a result provide an attractive force, which is sufficient to allow the retention of the gold nanoparticles following the addition of DDT. The corresponding comparison of the predicted and experimental coverage of gold nanoparticles following the addition of DDT is shown in Figure 12b.

Again, the good agreement between the theoretical prediction of the model and the experimental results provides important insights into the nature of the interactions which act between TOAB-stabilized gold nanoparticles and alkylthiol-modified MWCNTs following the addition of DDT, especially in view of the competition between the two strong interactions (i.e., gold nanoparticles covalently adsorbed at the surface of alkylthiol-modified MWCNTs, DDT adsorbed at the surface of gold nanoparticles).

In the case of MEA-MWCNTs, it is believed that the addition of DDT results in the adsorption of DDT molecules at the

exposed outer surface of the TOAB-stabilized gold nanoparticles. However, the covalent gold−thiol bonds between the MEA-MWCNTs and the gold nanoparticles are supplemented by a short-range charge transfer interaction between the MWCNTs and the gold nanoparticles which results in a combined attractive force which is strong enough to resist the desorption of the nanoparticles due to the adsorption of DDT.

In addition, the close approach that the short chain length (C_2SH) of the MEA ligands facilitates between the gold nanoparticles and the surface of the MWCNTs is believed to create a region between the materials, which is sterically demanding for the approach of DDT molecules. In this way, DDT molecules would not be able to penetrate this region and adsorb to the underside of the nanoparticles, thus allowing the gold nanoparticles to be cleaved from the surface of the MWCNTs.

Consequently, gold nanoparticles were found to remain adsorbed at the surface of the MEA-MWCNTs, as may be seen from Figure 11b. The coverage of nanoparticles was found to be 91%, which gives a clear indication that a strong driving force for nanoparticle adsorption is present at the surface of the MEA-MWCNTs. It is worth noting that the model predicts a coverage of approximately 15% for an alkylthiol chain length corresponding to C_3SH. The substitution of TOAB by DDT is favorable in this case; however, the DDT-stabilized gold nanoparticle can remain at the surface of the MWCNT as a result of a van der Waals attractive force. For longer chains, the repulsion is too strong and nanoparticles are maintained at relatively large distances from the MWCNTs; that is, repulsive interaction and zero coverage are predicted.

Results for the cases of MHO- and MUDO-MWCNTs support this prediction, as the coverage of nanoparticles in both cases was found to be 1%. In both cases, it is believed that the addition of DDT results in the adsorption of DDT molecules at the surface of the gold nanoparticles in far greater numbers than there are MWCNT-bound thiols. Consequently, the DDT molecules replace the MWCNTs-bound thiols and the nanoparticles are cleaved from the surface of the MWCNTs. In particular, this is made possible by the distance of separation between the gold nanoparticles and the surface of the MWCNTs on account of the steric barrier of the C_6 and C_{11} alkyl chains of the MHO and MUDO molecules. In addition, it is believed that, at such distances, any charge transfer or van der Waals contribution between the materials is insufficient to prevent the nanoparticles from moving away from the surface of the MWCNTs.

On the basis of the theoretical and experimental results discussed above, it is evident that the contributions of distance dependent attractive forces, in particular the charge transfer and van der Waals attraction, have significant implications on the retention of the gold nanoparticles adsorbed at the surface of the alkylthiol-modified MWCNTs. In particular, the charge transfer interaction is believed to be a crucial factor which supplements the covalent interactions only at short distances between the TOAB-stabilized gold nanoparticles and the surface of the alkylthiol-modified MWCNTs, thus providing sufficient attractive character for the nanoparticles to remain adsorbed. This evidence further supports the assertions and predictions of the model concerning the interactions between TOAB-stabilized gold nanoparticles and alkyl- and alkylthiol-modified MWCNTs.

Conclusions

A theoretical model has been developed to provide a detailed description of the interactions (charge transfer, van der Waals, osmotic, elastic, nonelastic, and covalent) between alkyl- and alkylthiol-modified MWCNTs and TOAB-stabilized nanoparticles. The model has also been used to predict the coverage of gold nanoparticles following the combination of the materials in solution. Comparison between the predictions of the theoretical model and the experimental results has allowed, for the first time, a quantitative description of the interactions between these materials.

Specifically, in the case of alkyl-modified MWCNTs, following their combination with TOAB-stabilized gold nanoparticles, it has been shown that the length of the alkyl chains at the surface of the MWCNTs is a controlling parameter of the adsorption of the nanoparticles (as the length increases, the coverage decreases). On the other hand, for alkylthiol-modified MWCNTs, the high degree of coverage of gold nanoparticles at their surface remains constant irrespective of the length of the alkylthiol chain.

It has also been shown that, following the combination of unmodified, alkyl-modified, and alkylthiol-modified MWCNTs with TOAB-stabilized gold nanoparticles, the addition of DDT results in desorption of the nanoparticles from the MWCNTs in all but the case of short-chain alkylthiol-modified MWCNTs. The series of experiments constitute an important test of the model, and good agreement of its prediction with the experimental findings further proves the validity of its assumptions.

Notably, the understanding of the MWCNT templated assembly of nanoparticles described in this paper has formed the basis for the establishment and control of more elaborate systems involving the templated assembly of nanoparticles at the surface of modified MWCNTs. An important insight is that under certain conditions the coverage of nanoparticles is very sensitive to the nature of surface modification and the environment, pointing the way to the rational design of CNT-based nanoscale devices with potentially widespread application.

Supporting Information Available: Images of unmodified MWCNTs, PA-MWCNTs, PTA-MWCNTs, OA-MWCNTs, DDA-MWCNTs, MEA-MWCNTs, MHO-MWCNTs, and MUDO-MWCNTs combined with TOAB-stabilized gold nanoparticles and discussions, equations, tables, schemes, and figures about ligand chain volume fraction, geometry of interactions, evaluation of interactions, calculation of A_{CNT} and A_p, binding energies, steric effects of the addition of DDT, combination of dodecanethiol-stabilized gold nanoparticles with unmodified, alkyl-modified, and alkylthiol-modified MWCNTs in solution, and characterization of modified MWCNTs, TOAB-stabilized gold nanoparticles, and DDT-stabilized gold nanoparticles. This material is available free of charge via the Internet at http://pubs.acs.org.

References and Notes

(1) Packan, P. A. *Science* **1999**, *285*, 2079.

(2) Parak, W. J.; Gerion, D.; Pellegrino, T.; Zanchet, D.; Micheel, C.; Williams, S. C.; Boudreau, R.; Le Gros, M. A.; Larabell, C. A.; Alivisatos, A. P. *Nanotechnology* **2003**, *14*, R15.

(3) Whitesides, G. M.; Mathias, J. P.; Seto, C. T. *Science* **1991**, *254*, 1312.

(4) Rotello, V. *Nanoparticles: Building Blocks for Nanotechnology*; Nanostructure Science and Technology; Kluwer Academic/Plenum Publishers: New York, 2003.

(5) Ohara, P. C.; Leff, D. V.; Heath J. R.; Gelbart W. M. *Phys. Rev. Lett.* **1995**, *75*, 3466.

(6) Niemeyer, C. *Angew. Chem., Int. Ed.* **2001**, *40*, 4128.

(7) Shipway, A. N.; Katz, E.; Willner, I. *ChemPhysChem* **2000**, *1*, 18.

(8) Katz, E.; Shipway, A. N.; Willner, I. Functionalized Metal Nanoparticles: Synthesis, properties and applications. In *Nanoscale Materials*; Liz-Marzan, L. M., Kamat, P., Eds.; Kluwer: Boston, MA, 2003.

(9) Daniel, M.-C.; Astruc, D. *Chem. Rev.* **2004**, *104*, 293.

(10) (a) Dai, H.; Wong, E. W.; Lieber, C. M. *Science* **1996**, *272*, 523. (b) Ren, Z. F.; Huang, Z. P.; Xu, J. W.; Wang, J. H.; Bush, P.; Siegel, M. P.; Provencio, P. N. *Science* **1998**, *282*, 1105. (c) Cassell, A. M.; Franklin, N. R.; Tombler, T. W.; Chan, E. M.; Han, J.; Dai, H. *J. Am. Chem.* Soc. **1999**, *121*, 7975. (d) Dai, H. *Acc. Chem. Res*. **2002**, *35*, 1035.

(11) Sun, Y.-P.; Fu, K.; Lin, Y.; Huang, W. *Acc. Chem. Res*. **2002**, *35*, 1096.

(12) Niyogi, S.; Hamon, M. A.; Hu, H.; Zhao, B.; Bhowmik, P.; Sen, R.; Itkis, M. E.; Haddon, R. C. *Acc. Chem. Res*. **2002**, *35*, 1105.

(13) (a) Frank, S.; Poncharal, P.; Wang, Z. L.; de Heer, W. A. *Science* **1998**, *280*, 1744. (b) Collins, P. G.; Arnold, M. S.; Avouris, P. *Science* **2001**, *292*, 706. (c) Tans, S. J.; Verschueren, A. R. M.; Dekker, C. *Nature* **1998**, *393*, 49. (d) Kong, J.; Franklin, N. R.; Zhou, C.; Chapline, M. G.; Peng, S.; Cho, K.; Dai, H. *Science* **2000**, *287*, 622.

(14) (a) McConnell, W. P.; Novak, J. P.; Brousseau, L. C., III; Fuierer, R. R.; Tenent, R. C.; Feldheim, D. L. *J. Phys. Chem. B* **2000**, *104*, 8925. (b) Mirkin, C. A.; Letsinger, R. L.; Mucic, R. C.; Storhoff, J. J. *Nature* **1996**, *382*, 607. (c) Storhoff, J. J.; Elghanian, R.; Mucic, R. C.; Mirkin, C. A.; Letsinger, R. L. *J. Am. Chem. Soc*. **1998**, *120*, 1959. (d) Fuhrer, M. S.; Nygård, J.; Shih, L.; Forero, M.; Yoon, Y. G.; Mazzoni, M. S. C.; Choi, H. J.; Ihm, J.; Louie, S. G.; Zettl, A.; McEuen, P. L. *Science* **2000**, *288*, 494. (e) Yao, Z.; Postma, H. W. C.; Balents, L.; Dekker, C. *Nature* **1999**, *402*, 273.

(15) Thelander, C.; Magnusson, M. H.; Deppert, K.; Samuelson, L.; Poulsen, P. R.; Nygård, J.; Borggreen, J. *Appl. Phys. Lett.* **2001**, *79*, 2106.

(16) Han, L.; Wu, W.; Kirk, F. L.; Luo, J.; Maye, M. M.; Kariuki, N. N.; Lin, Y.; Wang, C.; Zhong C.-J. *Langmuir* **2004**, *20*, 6019.

(17) Ye, X. R.; Lin, Y.; Wai, C. M. *Chem. Commun*. **2003**, 642.

(18) Fullam, S.; Cottell, D.; Rensmo, H.; Fitzmaurice, D. *Adv. Mater.* **2000**, *12*, 1430.

(19) Sainsbury, T.; Fitzmaurice, D. *Chem. Mater*. **2004**, *16*, 2174.

(20) Sainsbury, T.; Fitzmaurice, D. *Chem. Mater*. **2004**, *16*, 3780.

(21) Griffin, F.; Sainsbury, T.; Beecher, P.; Quinn, A.; Redmond, G.; Fitzmaurice, D.; to be submitted for publication.

(22) Zhang, J.; Wang, G.; Shon, Y.-S.; Zhou, O.; Superfine, R.; Murray, R. W. *J. Phys. Chem. B* **2003**, *107*, 3726.

(23) Korgel, B. A.; Fullam, S.; Connolly, S.; Fitzmaurice, D. *J. Phys. Chem. B* **1998**, *102*, 8379.

(24) Korgel, B. A.; Fitzmaurice, D. *Phys. Rev. Lett.* **1998**, *80*, 3531.

(25) Shah, P. S.; Husain, S.; Johnston, K.; Korgel, B. A. *J. Phys. Chem. B* **2002**, *106*, 12178.

(26) Hostetler, M. J.; Templeton, A. C.; Murray, R. W. *Langmuir* **1999**, *15*, 3782.

(27) Rabani, E.; Egorov, S. A. *Nano Lett.* **2002**, *2*, 69.

(28) Shah, P. S.; Holmes, J. D.; Johnston, K. P.; Korgel, B. A. *J. Phys. Chem. B* **2002**, *106*, 2545.

(29) Kitchens, C. L.; McLeod, M. C.; Roberts, C. B. *J. Phys. Chem. B* **2003**, *107*, 11331.

(30) Smitham, J. B.; Evans, R.; Napper, D. H. *J. Chem. Soc., Faraday Trans. 1* **1975**, *71*, 285.

(31) Evans, R.; Napper, D. H. *J. Chem. Soc., Faraday Trans. 1* **1977**, *73*, 1377.

(32) Vincent, B.; Edwards, J.; Emmett, S.; Jones, A. *Colloids Surf.* **1986**, *18*, 261.

(33) Israelachvili J. *Intermolecular & Surface Forces*, 2nd ed.; Academic Press: San Diego, CA, 1992.

(34) (a) Maxwell, A. J.; Brühwiler, P. A.; Nilsson, A.; Mårtensson, N.; Rudolf, P. *Phys. Rev. B* **1994**, *49*, 10717. (b) Hunt, M. R. C.; Modesti, S.; Rudolf, P.; Palmer, R. E. *Phys. Rev. B* **1995**, *51*, 10039. (c) Brust, M.; Kiely, C. J.; Bethell, D.; Schiffrin, D. *J. Am. Chem. Soc.* **1998**, *120*, 12367. (d) Corio, P.; Brown, S. D. M.; Marucci, A.; Pimenta, M. A.; Kneipp, K.; Dresselhaus, G.; Dresselhaus, M. S. *Phys. Rev. B* **2000**, *61*, 13202. (e) Czerw, R.; Foley, B.; Tekleab, D.; Rubio, A.; Ajayan, P. M.; Carroll, D. L. *Phys. Rev. B* **2002**, *66*, 033408.

(35) Fink, J.; Kiely, C. J.; Bethell, D.; Schiffrin, D. *Chem. Mater*. **1998**, *10*, 922.

(36) McConnell, H. M. *J. Chem. Phys*. **1961**, *35*, 508.

(37) Adams, D. M.; Brus, L.; Chidsey, C. E. D.; Creager, S.; Creutz, C.; Kagan, C. R.; Kamat, P. V.; Lieberman, M.; Lindsey, S.; Marcus, R. A.; Metzger, R. M.; Michel-Beyerle, M. E.; Miller, J. R.; Newton, M. D.; Rolison, D. R.; Sankey, O.; Schanze, K. S.; Yardley, J.; Zhu, X. *J. Phys. Chem. B* **2003**, *107*, 6668.

(38) Holmlin, R. E.; Haag, R.; Chabinyc, M. L.; Ismagilov, R. F.; Cohen, A. E.; Telfort, A.; Rampi, M. A.; Whitesides, G. M. *J. Am. Chem. Soc*. **2001**, *123*, 5057.

(39) Medeiros-Ribeiro, G.; Ohlberg, D. A. A.; Williams, R. S.; Heath, J. R. *Phys. Rev. B* **1999**, *59*, 1633.

(40) Thomas, P. J.; Kulkarni, G. U.; Rao, C. N. R. *Chem. Phys. Lett.* **2000**, *321*, 163.

(41) Chaki, N. K.; Aslam, M.; Gopakumar, T. G.; Sharma, J.; Pasricha, R.; Mulla, I. S.; Vijayamohanan, K. *J. Phys. Chem. B* **2003**, *107*, 13567.

(42) Durgun, E.; Dag, S.; Ciraci, S.; Gülseren, O. *J. Phys. Chem. B* **2004**, *108*, 575.

(43) Menon, M.; Andriotis, A. N.; Froudakis, G. E. *Chem. Phys. Lett.* **2000**, *320*, 425.

(44) Bhattacharjee, S.; Elimelech, M. *J. Colloid Interface Sci*. **1997**, *193*, 273.

(45) Meier, D. J. *J. Phys. Chem*. **1967**, *71*, 1861.

(46) Flory, P. J. *Principles of Polymer Chemistry*; Cornell University Press: New York, 1953.

(47) Tirado-Miranda, M.; Schmitt, A.; Callejas-Fernandez, J.; Fernandez-Barbero, A. *J. Chem. Phys.* **2003**, *119*, 9251.

(48) Thomas, K. G.; Zajicek, J.; Kamat, P. V. *Langmuir* **2002**, *18*, 3722.

(49) Sellers, H.; Ulman, A.; Shnidman, Y.; Eilers, J. *J. Am. Chem. Soc*. **1993**, *115*, 9389.

(50) Yourdshahyan, Y.; Rappe, A. M. *J. Chem. Phys.* **2002**, *117*, 825.

(51) Hiura, H.; Ebbesen, T.; Tanigaki, K. *Adv. Mater*. **1995**, *7*, 275.

(52) Liu, J.; Rinzler, A. G.; Dai, H.; Hafner, J. H.; Bradley, R. K.; Boul, P. J.; Lu, A.; Iverson, T.; Shelimov, K.; Huffman, C. B.; Rodriguez-Macias, F.; Shon, Y.-S.; Lee, T. R.; Colbert, D. T.; Smalley, R. E. *Science* **1998**, *280*, 1253.

(53) Brust, M.; Walker, M.; Bethell, D.; Schiffrin, D. J.; Whyman, R. J. *J. Chem. Soc., Chem. Commun.* **1994**, 801.

(54) (a) Ebbesen, T. W.; Ajayan, P. M.; Hiura, H.; Tanigaki, K. *Nature* **1994**, *367*, 519. (b) Zhao, B.; Hu, H.; Niyogi, S.; Itkis, M. E.; Hamon, M. A.; Bhowmik, P.; Meier, M. S.; Haddon, R. C. *J. Am. Chem. Soc.* **2001**, *123*, 11673. (c) Hu, H.; Zhao, B.; Itkis, M. E.; Haddon, R. C. *J. Phys. Chem. B* **2003**, *107*, 13838.

(55) Lu, K. L.; Lago, R. M.; Chen, Y. K.; Green, M. L. H.; Harris, P. J. F.; Tsang, S. C. *Carbon* **1996**, *34*, 814.

(56) Satishkumar, B. C.; Govindaraj, A.; Mofokeng, J.; Subbanna, G. N.; Rao, C. N. R. *J. Phys. B: At. Mol. Opt. Phys.* **1996**, *29*, 4925.

(57) Hiura, H. *Mol. Cryst. Liq. Cryst*. **1995**, *267*, 267.

(58) Ulman, A. *Chem. Rev.* **1996**, *96*, 1533.

(59) Saunders, A. E.; Sigman, M. B., Jr.; Korgel, B. A. *J. Phys. Chem. B* **2004**, *108*, 193.